

# Adsorption of Phosphorus on a Ru(0001) surface

## A density functional theory study

by

T. I. Beeker

to obtain the degree of Master of Science  
at the Delft University of Technology,  
to be defended publicly on September 2021 2:00 PM.

Student number: 4362616  
Project duration: September 15, 2020 – August 30, 2021  
Thesis committee: Dr. Ir. M. H. F. Sluiter, TU Delft  
Dr. J. Meyer, Universiteit Leiden, supervisor  
Dr. O. Moulτος, TU Delft  
Dr. P. Dey, TU Delft  
Daily supervisor: Dr. S. Hariharan, Universiteit Leiden  
Supervisor ASML: Dr. V. Hildenbrand, ASML

An electronic version of this thesis is available at <http://repository.tudelft.nl/>.



# Abstract

Interest in transition metal surfaces has grown in fields such as catalysts and semiconductors. Models of initial adsorption and growth of adsorbates are used to verify if certain structures are formed. Structural complexity and diversity of overlayers often determines this growth. Understanding the difference between a clean single crystal transition metal surface and adsorbate covered surfaces at the atomic scale are a first step. Characterization at atomic scale however can be challenging and help can come from electronic structure theory. Much is known about the overlayers of oxygen on a Ru(0001) surface, yet little research has been conducted in understanding the interaction between phosphorus and Ru(0001).

In this work the adsorption mechanism of phosphorus on a ruthenium (0001) is studied. Density functional theory (DFT) calculations were performed to find optimal adsorption sites on a Ru(0001) surface for P. The four high coordination positions were then used to form distinct combinations upon stacking layers. There it became evident that in the regime of first layers, the adhesion and stacking of adsorbate layers is governed by the Ru(0001) stacking order and highest probable coordination sites on the surface. Upon stacking more layers, the adsorbate layer follows a pattern of 'on top' stacking with alternating layer heights. The bond distances and lack of electron transfer show a tendency to form P-P bi-layers. Binding energies within the P-P bilayer (intra-bilayer) are stronger than binding energies between successive bi-layers (inter-bilayers). Latter one being dominated by VanderWaals forces. A minimal analytical sum of binding interactions is proposed to the surface and bilayer energies showing an accurate description of the DFT results. Bilayer formation and weak inter-bilayer interactions indicate the possibility of formation of two-dimensional phosphorene structures. At last as a point for future work possible supercells are constructed and tabulated that could accommodate adhesion of phosphorene (oxide) structures with minimal strain.



# Acknowledgements

I would like to thank Dr. Seenivan Hariharan for his patience and time to learn me all about DFT and how to apply it. Further I would like to thank Dr. Jörg Meyer for the discussions had and critical looks at the reporting. I would like ASML and specifically Volker Hildenbrand and Daniele Stradi for giving me this opportunity and their support of the project within the team. Lastly I would like to thank Marcel Sluiter showing possible directions when needed and everyone in the committee to have taken time to look at and listen to the work of the project.



# Contents

0.1 List of abbreviations . . . . .	ix
<b>List of Figures</b>	<b>xi</b>
<b>List of Tables</b>	<b>xiii</b>
<b>1 Introduction</b>	<b>1</b>
1.1 Motivation . . . . .	1
1.2 Previous work and ongoing work . . . . .	3
1.3 Knowledge gap . . . . .	3
1.4 Research aim . . . . .	3
1.5 Scope . . . . .	4
<b>2 Theoretical background and computational methods</b>	<b>5</b>
2.1 Cabrera-Mott model . . . . .	5
2.2 Electronic Structure Calculation . . . . .	6
2.3 Density functional theory (DFT) . . . . .	7
2.3.1 Exchange correlation functionals . . . . .	8
2.3.2 Dispersion . . . . .	9
2.4 Functionals used in this study . . . . .	9
2.4.1 PBE . . . . .	9
2.4.2 PBE+D3 . . . . .	9
2.4.3 vdW-DF2 . . . . .	9
2.5 Computational details . . . . .	10
2.5.1 Binding Energy . . . . .	10
2.5.2 DFT calculations . . . . .	10
2.5.3 Bader charge analysis . . . . .	11
<b>3 Properties of ruthenium and phosphorus</b>	<b>13</b>
3.1 Ruthenium . . . . .	13
3.2 Bulk Phosphorus . . . . .	13
3.3 Phosphorene . . . . .	14
3.3.1 Phosphorene oxides . . . . .	15
3.3.2 Discussion and conclusion . . . . .	15
3.4 Phosphorus oxides . . . . .	16
3.4.1 Phosphorus pentoxide (P <sub>2</sub> O <sub>5</sub> ) . . . . .	16
3.4.2 Phosphorus trioxide (P <sub>2</sub> O <sub>3</sub> ) . . . . .	16
3.4.3 Discussion and conclusion . . . . .	17
3.5 Ru(0001)-X, X = Si, O, S, N and C . . . . .	17
3.5.1 Silicon/Silica . . . . .	17
3.5.2 Oxygen . . . . .	17
3.5.3 Sulphur . . . . .	18
3.5.4 Nitrogen . . . . .	19
3.5.5 Carbon . . . . .	19
3.5.6 Discussion and conclusion . . . . .	19
<b>4 Results and Discussion</b>	<b>21</b>
4.1 Bulk phosphorous oxides . . . . .	21
4.2 Ruthenium (0001) surface . . . . .	23
4.3 Geometric fit of phosphorous oxides on a Ru(0001) surface . . . . .	25
4.3.1 Fit of 2D structures . . . . .	25

---

4.4	Reference states of the adsorbate . . . . .	27
4.4.1	Atoms in a box . . . . .	27
4.4.2	Free-standing phosphorus monolayers . . . . .	28
4.5	Monolayer adsorption . . . . .	29
4.5.1	Coverage . . . . .	30
4.6	Multilayer adsorption . . . . .	32
4.6.1	Two layers . . . . .	32
4.6.2	Three and more layers . . . . .	34
4.6.3	Energetics . . . . .	36
4.6.4	Structure . . . . .	37
4.7	Phosphorus bilayers . . . . .	38
4.7.1	Intra and interlayer bonding . . . . .	39
4.7.2	SB2M-formula . . . . .	43
<b>5</b>	<b>Conclusions, Summary and Outlook</b>	<b>47</b>
5.1	Conclusions . . . . .	47
5.2	Summary . . . . .	47
5.3	Outlook . . . . .	48
<b>6</b>	<b>Appendix</b>	<b>49</b>
6.1	Experimental techniques . . . . .	49
6.2	A 2D materials fit . . . . .	49
	<b>Bibliography</b>	<b>53</b>

## **0.1. List of abbreviations**

---

AES	Auger Electron Spectroscopy
ARPES	Angle-Resolved Photoemission Spectroscopy
BP	Black Phosphorus
DFT	Density Functional Theory
DFT-D	Density Functional Theory Dispersion (corrected)
EUV	Extreme UltraViolet
GGA	Generalized Gradient Approximation
HCP	Hexagonal Close Packed
HDS	hydrodesulfurization
HDO	hydrodeoxygenation
HER	Hydrogen Evolution Reaction
HF	Hartree-Fock
KS	Kohn-Sham
KS-DFT	Kohn-Sham Density Functional Theory
LDA	Local Density Approximation
LEED	Low-Energy Electron Diffraction
PAW	Projected Augmented Wave
PBE	Perdew-Burke-Ernzerhof
STM	Scanning Tunneling microscopy
TDS	Thermal Desorption Spectroscopy
UHV	Ultra High Vacuum
UPS	Ultraviolet photoelectron spectroscopy
VASP	Vienna Ab Initio Simulation Package
vdW	van der Waals
XC	exchange and correlation (functional)
XPS	X-ray Photoelectron Spectroscopy
XRD	X-ray diffraction

# List of Figures

1.1	schematic figure showing the path of EUV-radiation reflected and altered by mirrors inside an NXE lithography machine. . . . .	2
3.1	Hexagonal structure showing parameters a and c from [64] . . . . .	13
3.2	crystal structures of allotropes of phosphorus. (a) White phosphorus, (b) Red phosphorus (c) Violet phosphorus and (d) Black phosphorus. Images from Martin Uhrin [93] . . . . .	14
3.3	Side and top view of the two-dimensional (2d) phosphorene. . . . .	15
3.4	Computed unit cell of $\sigma'(P_2O_5)_\infty$ . Seen along the a, c and b axis in (a), (b) and (c) respectively. (d) Shows the polyhedral projection. . . . .	16
3.5	Computed unit cell of $P_2O_3$ with the unit cell in (a) and the cage structure in shown in (b). . . . .	17
3.6	Ru sites shown schematically. . . . .	18
3.7	adsorbed atoms (H,O,N,S,C on a Ru(0001) surface from [40] . . . . .	19
4.1	Slab models and 4-Layer asymmetric slab with 15 Å vacuum above the slab (a) and a 7-Layer symmetric slab surrounded by 12.5 Å vacuum on both sides (b) . . . . .	24
4.2	Area fit of a phosphorene ( $P_4$ ) unit area over different Ru(0001) supercell areas. Supercell combinations where rest strain to the closest integer (either compression or tension) is less than 10% of the unit area are denoted in green. . . . .	25
4.3	Area fit of a phosphorene ( $P_4O$ ) unit area over different Ru(0001) supercell areas. Supercell combinations where rest strain to the closest integer (either compression or tension) is less than 10% of the unit area are denoted in green. . . . .	26
4.4	Area fit of a phosphorene ( $P_4O_2$ ) unit area over different Ru(0001) supercell areas. Supercell combinations where rest strain to the closest integer (either compression or tension) is less than 10% of the unit area are denoted in green. . . . .	26
4.5	Area fit of a phosphorene ( $P_4O_{10}$ ) unit area over different Ru(0001) supercell areas. Supercell combinations where rest strain to the closest integer (either compression or tension) is less than 10% of the unit area are denoted in green. . . . .	26
4.6	Different electronic configurations for phosphorus and oxygen considered here. The respective ground states (according to Hund's rule) are shown on the left, and an electronically excited state is shown on the right. . . . .	27
4.7	Final energy of a P monolayer plotted for different spin states . . . . .	29
4.8	Top view of 2x2 cell with a single P atom on an hcp site on the Ru(0001) surface. This corresponds to $\theta = 0.25$ ML . . . . .	30
4.9	Top view of 2x2 cell with two P atoms on an hcp site on the Ru(0001) surface. This corresponds to $\theta = 0.5$ ML . . . . .	30
4.10	Top view of 2x2 cell with a three P atoms on an hcp site on the Ru(0001) surface. This corresponds to $\theta = 0.75$ ML . . . . .	30
4.11	Top view of 2x2 cell with four P atoms in on hcp site on the Ru(0001) surface. This corresponds to $\theta = 1$ ML . . . . .	30
4.12	Coverage dependence on a ruthenium surface . . . . .	31
4.13	16 High coordination site positions with an oxygen atom above a phosphorus atom above the Ru(0001) surface. The ruthenium atoms are shown in green, the phosphorus in orange and the oxygen atoms in red. . . . .	32
4.14	16 High coordination site positions with a phosphorus atom above an oxygen atom above the Ru(0001) surface, the ruthenium atoms are shown in green, the phosphorus in orange and the oxygen atoms in red. . . . .	33
4.15	Final energy of system in VASP plotted against distance of third adsorbate atom above the second one in the situation of Ru-P-O-P. . . . .	35
4.16	Charge transfer between layers in a system of 10 layers P on top of Ru(0001) [ $e^-$ ] . . . . .	36

4.17 Adsorption energies per atom on a Ru(0001) surface. The x-axis represents the amount of P-layers on the surface. . . . .	37
4.18 Distance between layers of P on Ru(0001). With $d_{01}$ being the distance between the top 2 atoms, and $d_{12}$ the distance between the second and third atom from the top. The distances labeled with dots represent an intra-bilayer distance. The distances labeled with triangles represent an inter-bilayer distance. Values are made with the XC-functional being PBE. . . . .	38
4.19 Distinction between inter- and intra-bilayers and their bond lengths D and d respectively.	39
4.20 Binding energy and intra-bilayer distances for different inter-bilayer bond lengths using the PBE functional. . . . .	39
4.21 Schematic description of situation of bilayering in phosphorus layers. Distance D shown in black and distance d shown in red. Situation A shows a single bilayer, B the optimal positions of two bilayers, and C the long distance position of two bilayers. . . . .	40
4.22 Binding energy and intra-bilayer distances for different inter-bilayer bond lengths using the PBE functional with the D3 correction. . . . .	40
4.23 Binding energy and intra-bilayer distances for different inter-bilayer bond lengths using the vdW-DF2 functional. . . . .	41
4.24 Bilayer schematic showing intra-bilayer bond d. . . . .	41
4.25 Binding energy curves of P-bilayers using PBE, PBE+D3 and vdW-DF2. . . . .	42
4.26 schematic showing boundary of simulation of inter-bilayers D. . . . .	42
4.27 Binding energy curves between 2 P bilayers using three methods. . . . .	43
4.28 Amount of inter-bilayers taken into account using methods A and B. . . . .	44
4.29 Difference between simulations and SB2M(+) method for systems of P overlayers on the surface. . . . .	45
4.30 Adsorption energies of VASP simulation (dots) and SB2M(+) formula (lines). . . . .	45
6.1 Phosphorene . . . . .	50
6.2 phosphorene oxide P4O . . . . .	50
6.3 phosphorene oxide P4O2 . . . . .	50
6.4 phosphorene oxide P4O6 . . . . .	51
6.5 phosphorene oxide P4O7 . . . . .	51
6.6 phosphorene oxide P4O8 . . . . .	51
6.7 phosphorene oxide P4O9 . . . . .	52
6.8 phosphorene oxide P4O10 . . . . .	52

# List of Tables

4.1	Unit cell lengths, volumes and total energy for phosphorus pentoxide $P_2O_5$ . . . . .	21
4.2	Phosphorus pentoxide $P_2O_5$ unit cell lengths and volumes compared to Ainsworth et al. [2] . . . . .	22
4.3	Unit cell lengths, volumes, total energy and beta angle for phosphorus trioxide $P_2O_3$ . . . . .	22
4.4	Atomization energies of phosphorus pentoxide $P_2O_5$ . . . . .	23
4.5	Atomization energies of phosphorus trioxide $P_2O_3$ . . . . .	23
4.6	Final energy of a 7-layer Ru slab with different k-point sampling . . . . .	23
4.7	Final energies for 4-layer ruthenium surface after relaxing 2,3 or 4 layers. . . . .	24
4.8	Ground state energy of phosphorus in electron volts . . . . .	28
4.9	Ground state energy of single atom of phosphorus . . . . .	28
4.10	Ground state energy of single atom of oxygen . . . . .	28
4.11	Adsorption energies of phosphorus on 4 high coordination sites in eV . . . . .	29
4.12	Adsorption energies of oxygen on 4 high coordination sites in eV . . . . .	30
4.13	Coverage dependence of adsorption for phosphorus and oxygen atoms on a ruthenium surface . . . . .	31
4.14	Coverage dependence compared to Stampfl. et al. [85] . . . . .	31
4.15	Adsorption energies per atom for 16 combinations of 2 atoms in 4 high coordination sites in eV . . . . .	32
4.16	Adsorption energies per atom for 16 combinations of 2 atoms in 4 high coordination sites in eV including dispersion . . . . .	33
4.17	Adsorption energies per atom for 16 combinations of one phosphorus atom on one oxygen atom in 4 high coordination sites in eV . . . . .	33
4.18	Adsorption energies per atom for combinations of 2 atoms in 4 high coordination sites in eV using P and O atoms, without lateral constraints. . . . .	34
4.19	Adsorption energies per atom for 16 combinations of 2 atoms in 4 high coordination sites in eV using 2 phosphorus atoms. . . . .	34



# 1

## Introduction

Devices including chips are widespread. Everything from computers, phones, appliances and cars are full of them. In recent times the field of semiconductors has increased rapidly to one of the most important industries worldwide, with a total sales revenue of over 500 billion dollar [21]. With increasing demand for data and electronics, the amount of chips increases as well. With Moore's law nearing its end [99], optimization and further reduction of structure sizes on chips is becoming more crucial than ever.

One of the most crucial elements determining the size of chips that can be produced is the lithography machine needed in the process to produce the chip. The state-of-the-art technology to defining resolution of imaging in the process of lithography is Extreme Ultra-Violet (EUV) radiation [92]. Mirrors that reflect and alter the path of radiation have to be passive to both the radiation as to background gases and particles. In semiconducting industry the ruthenium is used as a capping layer for surfaces of the mirrors. Its low reactivity to many materials makes it suited to reflect radiation without unwanted chemical processes to appear. Adhesion of atoms to the surface however is something that in many cases can not simply be avoided. Therefore fundamental understanding of the adhesion is needed to understand why adhesion takes place and what can be done to avoid it or work around it.

### 1.1. Motivation

The new NXE series lithography machines currently in use at ASML are known for having the highest [76] resolution for making chips. This is a complicated process in which a beam from a laser source is reflected and manipulated over a series of mirrors to hit a minuscule droplet of tin (with a diameter of 20  $\mu\text{m}$  [106]) in order to generate the EUV radiation with a wavelength  $\lambda = 13.5 \text{ nm}$ . The entire process of building the lithography machine occurs in a clean environment (ISO1) and the machine operates in high vacuum conditions. It is, however, unavoidable to have some form of contamination, be it from the machine parts itself or from outside, which, at some point interacts with the mirrors. In figure 1.1 the path of EUV is shown moving between mirrors. To extend the lifetime of Mo/Si mirrors a few monolayer thick capping of Ru is used [66]. The ruthenium capping however will also degrade and or react to other compounds present.



Figure 1.1: schematic figure showing the path of EUV-radiation reflected and altered by mirrors inside an NXE lithography machine.

Extensive research is being done to investigate what compounds will adhere to the lithography machine's mirrors and its effects. Experimental research is reaching limits in terms of accuracy, cost and labor intensity for this situation. Classical experimental methods such as microscopy (scanning electron (SEM), or transmission electron (TEM), Scanning Tunneling Microscopy (STM)), X-ray diffraction (XRD) or X-ray photo-electron spectroscopy (XPS) are all invasive methods that require the manufacturing process to stop and mirrors to be taken out. The downtime in such a procedure will be in the order of hours to days. Most characterisation methods are unable to or have severe difficulty in reaching atomic limits needed to clarify the fundamental process of adhesion on a surface. A different approach to investigate is to model the system computationally. One of the possible atomic species present in the chamber would be phosphorus. The surface layer of the mirror consists of a ruthenium capping. Among a set of other gases present in the chamber, it can also be expected to have some contamination of oxygen present. The mechanisms of adsorption and reaction between oxygen and ruthenium are studied in greater detail ([55],[45],[56],[104], [47], [91],[7], [36], [109], [75], [35], [85], [84][9], [10]), there is however no such description for the adhesion of phosphorus to a Ru surface. This report is a study to investigate the structures that elemental phosphorus could form when adsorbed to the ruthenium surface.

Up till this moment, efforts have been put to reduce the downtime of lithography machines and thus operational costs by mainly running a clean and controlled process. To have a better understanding of the fundamental reactions possibly happening inside the ultra high vacuum environment of the lithography machines, it is important to also model the possible interactions using electronic structure calculations. For different metal-oxides there is a clear theory and model of growth such as iron [71], aluminium [6], [71] and nickel [74]. In the case of oxygen as adsorbate these can also be compared to the classical continuum model of Cabrera and Mott (CM) [14]. There are publications about the interaction between ruthenium and other materials such as for instance oxygen [85] or silica[27, 28, 89]. The interaction between elemental phosphorus or phosphorous oxides and a ruthenium surface is not reported till date. Since the system of P adsorption on Ru(0001) is not yet studied, the logical steps would be to investigate the properties of phosphorus, ruthenium and systems similar to P on Ru(0001). The way ruthenium and phosphorus will react to each other can partly be derived from looking at the binary phase diagram. Looking at adsorption of elements of similar size or energetic behaviour as P is a logical step. Nitrogen and arsenic, like P, belong to the nitrogen group of elements and have the same amount of valence electrons. Silicon and sulphur are atomically close to phosphorus and have similar atomic masses.

This document is structured as follows: chapter 2 will go over theory and methods used to investi-

gate. In section 2.2 theoretical background of electronic structure calculations and models of oxidation are summarised. Section 2.5 details the computational settings used to obtain the results in this report. Throughout this work the Vienna Ab Initio Suite (VASP) has been used to perform Density Functional Theory (DFT) calculations. Chapter 3 covers the literature related to the system. In chapter 4 the results of the study are listed and explained. In section 4 a study of bulk structures is shown, section 4.3 elaborates on the computational sizes needed to model two-dimensional phosphorene (oxides) on a Ru surface. Section 4.4.1 describes the gas phase calculations of both phosphorus and oxygen. In section 4.5 monolayer adsorption results are shown for both oxygen and phosphorus. In section 4.6 multilayer adsorption and growth are investigated. Section ?? describes the method of growth and section 4.7 the energies related to bilayers. Lastly section 4.7.2 shows how the growth can be estimated using a summation of energies. In chapter 5 conclusions, summary and the outlook can be found.

## 1.2. Previous work and ongoing work

The main body of this work is a follow up on previous findings of adsorption of oxygen on Ru(0001) in the low coverage regime carried out at the theoretical chemistry group of Leiden Institute of Chemistry. All simulations thereof were performed using using DFT with and without vdW correction. Experimental work is carried out in the laboratories of ASML to further detect possible compounds that affects the mirrors inside the EUV chamber.

## 1.3. Knowledge gap

The combination of ruthenium and phosphorus are mainly used in the fields of catalysis and the semiconductor industry. The form in which it is used is however different. As a catalyst ruthenium surfaces doped with phosphorus can be used for the hydrogen evolution reaction (HER)[110],[62],[57] or for hydrodesulfurization (HDS) or hydrodeoxygenation (HDO) [54]. This report is about the adsorption of P on Ru which is not described in the field of catalysis. No scientific literature is found reporting of adsorption of P on a Ru(0001) surface. There is however clear reporting mainly on the system involving adsorption of O on Ru(0001). Using DFT/GGA with dispersion taken into account one can model the adsorption of elemental P on a Ru(0001) surface rather well. There are however pitfalls in the calculation strategy as there is no functional that is perfectly suited at describing the metallic character of Ru and the vanderWaals forces likely present when dealing with P. For this it is advised to screen functionals first using both a Ru surface and a P based compound separately. This method can give a result that is within boundaries of DFT calculations and can predict initial adsorption to the Ru(0001) surface at relatively low computational cost. In order to accurately describe initial adsorption and growth while keeping computational cost to a minimum it makes sense to limit the system size by using a small computational cell modelling one adatom over the surface. By keeping the computational setup small, monolayer behaviour can be modelled within a suitable time frame. One does have to keep in mind that the low-cost small systems are limited in representing structures that form over multiple atoms. This means preferred adsorption sites can be predicted, yet corrugated structures as phosphorene are not able to form.

## 1.4. Research aim

In this work, the goal is to get insights into the adsorption of phosphorus on a Ru(0001) surface. The study will focus on initial adsorption and make a first step towards modelling multi-layer growth. Effects of different functionals with and without vdW corrections will be studied and comparisons will be made to the results from well-studied O on Ru(0001) surface. Finally, the growth of phosphorous multi-layers will be studied and compared with the well-established Cabrera-Mott model.

This leads to the main research question:

**How does phosphorous overlayers adsorb on a Ru(0001) surface, and what is the mechanism of multi-layer growth?**

The question can be divided into two parts: the initial adsorption of P atoms to the surface, and the growth mechanism. Two sub-questions can be formulated from there:

1. What are the preferred adsorption sites for P overlayers on the Ru(0001) surface and how strongly do they bind?

2. How will adhesion of P overlayers continue to grow and what is the underlying mechanism?

## 1.5. Scope

The scope of the project defines the boundaries of this study.

- Preparing a computational setup through Python/ASE to model systems using VASP.
- Screen functionals for their use in modelling a Ru(0001) surface and bulk  $\text{PO}_x$ .
- Model monolayer adsorption of P on Ru(0001).
- Model growth of overlayers of P on Ru(0001).
- Validate outcomes to adsorption from literature and growth from CM-model and literature.

Outside the scope of this project fall:

- Validation of outcomes to experimental results.
- Modelling of adsorption in larger unit cells that allow to describe low coverage and/or lattice mismatch.
- Modelling of growth behaviour of oxides on a Ru(0001) surface.

# 2

## Theoretical background and computational methods

Throughout literature various methods are used to study adsorption. Since the study of chapter 4 will consist of electronic structure calculations in the form of DFT, it is key to understand which methods are used and how they relate to each other. Experimental methods have also been used to study adsorption in literature. Of those methods it is relevant how they behave and more importantly how they compare to computational results.

### 2.1. Cabrera-Mott model

Prediction of growth of oxides can be divided into two regimes: thin film and thick film. In principle, every oxidising metal will, given enough time and energy, go through both regimes. There are, however, different approaches that distinguish both regimes and to model them. In the thick film regime, electric charges be described as continuous space charge layers as opposed to charges of individual atoms. The thick film is mainly described by Wagner's theorem based on the linear diffusion equation for charged particles [98]. The thin-film regime is more relevant for this project as we study the first few layers of phosphorous multi-layer formation. Thin-film oxidation of metals can be described by the Cabrera-Mott (CM) model[14].

Passivation of the formed oxide layer occurs due to electrons at the Fermi level of the metal surface traversing through the oxide film. Anions are formed at the surface of the oxide, which together with the positive cations on the metal-oxide interface generate an electric potential (the Mott potential  $E_b$ ) lowering the barrier for movement of anions and/or cations through the oxide. During growth, the Mott potential lowers until movement of the anions and cations effectively drops to 0 and a passive layer with thickness  $X$  is formed. The reaction of oxidising the metal is assumed to be in equilibrium with equilibrium constant  $K$ . The driving force ( $\Delta G_0$ ) of the potential field between the metal and the outer layer of the oxide (with  $\Phi_m$  being the electric potential of the metal and  $\Phi_{ox}$  the electric potential of the oxide) explains why the behaviour of oxidation will also happen at sufficiently low temperatures (where the thermal energy  $k_b * T$  is not sufficient for the process of oxidation to happen spontaneously without another driving force ( $\Delta G^0$ )). The equilibrium constant The potential driving the ionic motion through oxide film is the Mott potential,  $E_b$ :

$$E_b = 1/e(\Phi_m - \Phi_{ox}) \quad (2.1)$$

The potential is calculated from the assumption that the adsorbed layer of ions is in equilibrium (with equilibrium constant  $K$ ) with the gas layer above. The activity of the oxygen dimer activity is denoted by  $a(O_2)$ . These combined form:

$$K = \frac{a(O^{2-})}{a(O_2)^{1/2} a(e)^2}. \quad (2.2)$$

With  $K$  related to thermodynamics through:

$$K = e^{\frac{-\Delta G^0}{kT}}. \quad (2.3)$$

The excess oxygen ions ( $n_0$ ) can be expressed based on the total number of oxygen ions ( $N_s$ ), activity of the oxygen ions and thermodynamics.

$$n_0 = N_s a(O_2)^{1/2} e^{\left[-\frac{\Delta G^0 + 2e\Delta\Phi}{kT}\right]}. \quad (2.4)$$

The excess oxygen ions  $n_0$  forming the surface charges can also be expressed as a capacitor with dielectric permittivity ( $\epsilon$ ) leading to:

$$n_0 = \frac{\epsilon\epsilon_0\Delta\Phi}{2eX}. \quad (2.5)$$

$X$ , in this case, is the oxide film thickness. The last two equations together can express the Mott potential:

$$\frac{2e\Delta\Phi}{kT} + \ln\left[\frac{2e\Delta\Phi}{kT}\right] = -\frac{\Delta G^0}{kT} + \ln\left[\frac{4e^2 N_s a(O_2)^{1/2} X}{kT\epsilon\epsilon_0}\right]. \quad (2.6)$$

As the Mott potential difference  $e\Delta\Phi/kT$  will in most cases be above unity, the equation from above can be simplified to:

$$\Delta\Phi = -\frac{\Delta G^0}{2e} + \frac{kT}{2e} \ln\left[\frac{4e^2 N_s a(O_2)^{1/2} X}{kT\epsilon\epsilon_0}\right]. \quad (2.7)$$

The Cabrera-Mott model is meant to predict the passivating oxidation of metal surfaces. The method takes into account the Mott potential formed due to adsorption and its influence on transfer of cations or anions. This is however only applicable to the situation of only metal- $O_2$  combinations. For phosphorus, in its elemental state or any other form, it is unclear whether the formation of multi-layers follows the Cabrera-Mott type model or not. Computational investigations along these lines will be a part of this work.

## 2.2. Electronic Structure Calculation

Electronic structure calculations are widely used for determining the structure and energetics of a system. In this case, the system consists of a Ru(0001) surface in the solid phase and phosphorus and oxygen atoms in the gas phase.

The nuclei of atoms are treated as fixed particles from the Born-Oppenheimer approximation. Nuclei of atoms are much heavier than the electrons surrounding them. Since the difference in mass of the nuclei and the electrons is around 3 orders of magnitude, one can make the assumption that an electron will respond so much faster than the nuclei to its surroundings. Therefore, the nuclei can be considered static compared to electrons. This generates a static external potential  $V_{eN}$  in which the electrons are moving. The electrons have a kinetic energy  $T_e$ . The electron-electron interaction energy is denoted by  $U_{ee}$ . The three terms form the Hamiltonian  $\hat{H}$  acting on the wavefunction  $\Psi$ .

$$\hat{H}\Psi = [\hat{T}_e + \hat{V}_{eN} + \hat{U}_{ee}] \Psi \quad (2.8)$$

The Hamiltonian of a multi-electron system can be defined as follows (2.9)

$$\left[ -\frac{\hbar^2}{2m} \sum_{i1}^N \nabla^2 + \sum_{i1}^N V(\mathbf{r}_{i1}) + \sum_{i1}^N \sum_{j<i}^N U(r_i, r_j) \right] \Psi = E\Psi. \quad (2.9)$$

The electron mass is represented by  $m$ . The three operators define the kinetic energy of the electrons, the interaction energy between the electrons and the atomic nuclei and the interaction between electrons respectively.  $\Psi$  in this case is the electronic wavefunction, representing the spatial coordinates (and spin) of all  $N$  electrons.  $E$  is the total energy. The first two operators are identical for any system with the same amount of electrons. The many-body problem of interacting electrons within the external potential can be reduced to a problem of non-interacting electrons moving in an effective potential. The effective potential can then be divided into coulomb interactions between the electrons and the exchange and correlation interactions. This is the foundation of Kohn-Sham density functional theory (KS-DFT), or simply DFT.

## 2.3. Density functional theory (DFT)

Density functional theory is a widely accepted and popular method for performing electronic structure calculations for the gas-solid systems. It has seen widespread application over the past two decades in multiple fields spanning among others: physics, chemistry and materials science[108]. A fundamental equations in electronic structure calculations using DFT are the mathematical theorems proved by Hohenberg and Kohn [42] and resulting equations by Kohn and Sham [49]. The first theorem proved by Hohenberg and Kohn is as follows:

*The ground state energy from Schrödinger's equation is a unique functional of the electron density.*

This link between the ground state energy and electron density is important since the ground state energy can be calculated from electron density, which reduces the many-body problem of  $N$  electrons with  $3N$  spatial coordinates back down to three spatial coordinates. The second theorem from Hohenberg and Kohn states:

*The electron density that minimizes the energy of the functional is the true electron density corresponding to the full solution of the Schrödinger equation.*

$$n(\mathbf{r}) \Rightarrow E \quad (2.10)$$

and the total energy is a functional of the density:

$$E = E[n(\mathbf{r})] \quad (2.11)$$

to be more specific, the electron density  $n(r)$  uniquely determines the external potential  $V_{eN}(r)$ . With a given external potential  $v(r)$  the electron density can be varied until a minimum in energy is found.

$$E \equiv \int V(r)n(r)dr + F[n(r)] \quad (2.12)$$

With  $F[n(r)]$  being the universal functional composed of the kinetic and electron-electron interactions:

$$F[n(r)] \equiv \langle \Phi | \hat{T} + \hat{U} | \Phi \rangle \quad (2.13)$$

The variational problem of minimising the energy functional  $E[n](r)$  can be solved by first considering there to be no electron-electron interaction only taking  $\hat{T}_e$  and an effective potential  $v_{eff}$  into account. This way the KS-equations of the non-interacting system can be derived yielding orbitals  $\phi_i$  that are the solution to the lowest energy:

$$\left[ -\frac{\hbar^2}{2m} \nabla^2 + v_{eff}(\mathbf{r}) \right] \phi_i(\mathbf{r}) = \epsilon_i \phi_i(\mathbf{r}) \quad (2.14)$$

Here  $\epsilon_i$  is the orbital energy corresponding to the orbital  $\phi_i$ .

These orbitals can then be used to reproduce the electron density of the previous many-body system.

$$n(\mathbf{r}) = \sum_{i=1}^N |\phi_i(\mathbf{r})|^2 \quad (2.15)$$

The effective potential used however is still not fully defined. It can be written as a function of the external potential  $V_{eN}$ , the electron-electron coulomb repulsion, and a potential considering exchange and correlation effects  $V_{XC}$ :

$$v_{eff}(\mathbf{r}) = V_{eN} + \int \frac{n(\mathbf{r}')}{|\mathbf{r} - \mathbf{r}'|} d^3\mathbf{r}' + V_{XC}[n(\mathbf{r})] \quad (2.16)$$

Both the Coulomb effect and the XC-potential  $V_{XC}$  are dependent on the electronic density. They will however through Equations 2.14 and 2.15 also yield electron densities. This shows the iterative process

of KS-DFT where an initial trial density has to be made, leading eventually to converged electron density and total energy. Those can then be used to derive e.g. forces, structure and lattice information.

This leaves one part left untouched. The XC-potential has not been fully defined. This is actually where most of the current research in KS-DFT studies are being done. The exchange-correlation functional is the main problem of most calculations as its exact and system-independent form is not formulated.

### 2.3.1. Exchange correlation functionals

Since there is no exact exchange-correlation functional ( $E_{xc}[n]$ ) and thus no exchange-correlation potential  $V_{xc}$  that can describe every system accurately, multiple approximations are used over time in calculations. Finding good approximations for  $E_{xc}[n]$  is still one of the greatest challenges in modern DFT. The exchange-correlation problem has a wide variety of approaches to find a functional that can accurately describe one or multiple classes of systems. This estimation can be done both in a bottom-up approach where the functional is built from physics alone or a top-down approach where semi-empirical values are introduced to accurately imitate experimental outcomes to describe. A mix of both can also be used. Historically the simplest possible approximation for  $E_{xc}$  the local-density approximation has shown surprising accuracy for the description of solid-state systems. The exchange-correlation potential is defined as the functional derivative with respect to the density of the exchange-correlation energy functional:

$$V_{xc}(r) = \frac{\delta E_{xc}[n(r)]}{\delta n(r)} \quad (2.17)$$

Local density approximation (LDA)

In a homogeneous electron gas, we assume the observed local electron density to be equal to the electron density at any place in the gas, since it is uniform. For this situation accurate solutions are available [17]. One can set the exchange-correlation potential at each position of a material to the known exchange-correlation potential of the uniform electron gas at the electron density observed at this position [111]:

$$V_{xc}(\mathbf{r}) = V_{xc}^{electron\ gas}[n(\mathbf{r})]. \quad (2.18)$$

Within this approximation, the electron density is constructed as the total of local electron densities at given points, therefore this is called the local density approximation (LDA). While LDA is still important for modern day DFT calculations, the method is insufficient for evaluating systems where the differences between electron densities change quickly over a dimension in the system. Such as is the case in non-metals, molecules or atoms adsorbed on a surface. In other words, the further the system differs from a uniform electron gas, the worse LDA will be at describing its behaviour.

Generalized gradient approximation (GGA)

Improving on the LDA, an overall better performing exchange-correlation approach is the generalized gradient approximation (GGA). Here not only the local density is taken into account, but also the gradient of it [111]:

$$E_{xc}[n] = \int f[n(\mathbf{r}), |\nabla n(\mathbf{r})|] d\mathbf{r}, \quad (2.19)$$

with density gradient  $\nabla n(\mathbf{r})$  as the functional derivative of density  $n(\mathbf{r})$  and  $f$  the analytical function. The GGA functional has been the method of choice for many applications over the past years due to its suitability at describing various systems where chemical bonding is important. The overall difference in results between the LDA or GGA based calculations is where LDA systems tend to higher binding energies with longer bond lengths, GGA based work tends to estimate larger bonds with smaller binding energies. While GGA works well for the metals, its applicability for the gas-solid interface is still under scrutiny. The difficult aspect of the Ru(0001)-P-O system under study is the different phases it consists of. Ruthenium being a metal it will have an electron density spread over a surface, whereas the possible adsorbates will have rather discrete energy levels. However, earlier DFT calculations for O adsorption on the Ru(0001) surface [85] have been successful in reproducing experimental results. DFT-based studies for interaction between phosphorus and Ru(0001) is not reported yet. For this reason, we have decided to use the GGA based functionals to study P/Ru(0001) system in chapter 4.

### 2.3.2. Dispersion

Long range interactions such as the van der Waals (vdW) forces are important while studying multilayer formation on metal surfaces. They are not taken into account in KS-DFT as the forces are not part of bound atoms. It is well known that layers of graphene in graphite is held together by long range vdW interactions. Along these lines, since phosphorous is known to form 2D structures like phosphorene, it becomes important to take vdW interactions into consideration when studying multilayer formation of phosphorous. Large polar systems also inhibit non-linear scaling of forces with respect to size giving rise to more challenges in modeling vdW interactions, because these interactions involve a large number of electrons [26, 31].

At the moment, two approaches of accounting for vdW interactions are prevalent for gas-surface systems. [86] In the first, the so-called the DFT+D approach, dispersion corrections are added to the Kohn-Sham DFT energies as correction terms, for example, Grimme's dispersion correction (D2, D3, D3(BJ) and D4) schemes [34] and Tkatchenko-Scheffler schemes [90]. In the other class, the dispersion energy correction terms are included in the self-consistent field (SCF) iterations, for example, vdW-DF form of functionals due to Langreth and Lundqvist [25]. vdW-DF based functionals have proven to be very well suited at describing phosphorene behaviour [69], [82]. DFT+D has proven to be good at describing phosphorus oxides [2] and Silica on Ru(0001) [63].

## 2.4. Functionals used in this study

### 2.4.1. PBE

The exchange correlation functional formulated by Perdew, Burke and Ernzerhof or PBE [78] is a widely used first-principles functional within the type of generalised gradient approximation functionals. Its popularity is mainly due to its relative success in describing different types of systems. The functional is semi-local, depending both on  $n(r)$  as well as  $\nabla n(r)$ . The PBE functional proved to be suitable at describing Ru(0001) surfaces in earlier work done in the Theoretical Chemistry group of Leiden University [8] as well as literature from the Stampfl and colleagues [85], [84]. The PBE functional is also proven to be a good overall functional for considering both surface and bulk properties of transition metals [96].

### 2.4.2. PBE+D3

Grimme and colleagues [34] proposed a correction method for van der Waals energies using DFT in the following equation:

$$E_{disp} = -\frac{1}{2} \sum_{i=1}^{N_{at}} \sum_{j=1}^{N_{at}} \sum_L^l (f_{d,6}(r_{ij}) \frac{C_{6ij}}{r_{ij}^6} + (f_{d,8}(r_{ij}) \frac{C_{8ij}}{r_{ij}^8}). \quad (2.20)$$

In this equation the  $C_{6ij}$  dispersion coefficients are geometry dependent, based on the local geometry around atoms  $i$  and  $j$ . In the method of Grimme [34] the damping follows the form of:

$$f_{d,n}(r_{ij}) = \frac{S_n}{1 + 6(r_{ij}/(S_{R,n}R_{0ij}))^{-\alpha_n}}. \quad (2.21)$$

Where  $S_R, S_n, \alpha_n$  are fixed damping parameters. With:

$$R_{0ij} = \sqrt{\frac{C_{8ij}}{C_{6ij}}}. \quad (2.22)$$

These correction based methods are more suitable at describing dispersion interactions through the use of effective pair potentials, but will lack the 'knowledge' how bonds may behave and compete when there are Van der Waals interactions present. To fully take these into account a fully self-consistent Van der Waals functional has to be used. The DFT-D setup can be used with the PBE functional and yield an improvement over the latter alone for the systems studied here (as shown in section 2.4.1).

### 2.4.3. vdW-DF2

One possible method of that does use full Self-Consistent Field (SCF) iterations in estimating a system where Van der Waals energies are likely present is using vdW-DF2 as a functional [25] [48]. Dion and

colleagues have shown that it allows to describe purely vdW-bound systems (rare gas and benzene dimers) for which LDA and GGA functional fail miserably. It uses the rPW86 exchange functional. In vdW-DF functionals the non-local correlation calculated by having the exchange-correlation energy taking the form:

$$E_{XC} = E_x^{GGA} + E_c^{LDA} + E_c^{nl}. \quad (2.23)$$

The exchange-correlation energy is formulated as a sum of the exchange energy from PBE. The local correlation energy is calculated using LDA and non-local correlation energies are accounted for separately. VDW-DF based functionals have proven to be very well suited at describing phosphorene behaviour [69].

## 2.5. Computational details

Above mentioned methods and approaches have to be translated to actual used settings in a computational setup.

### 2.5.1. Binding Energy

Adsorption energy ( $E_{ads}$ ) of atoms is the difference in energy when bound  $E_{final}$  compared to unbound. In the case of adsorption these two states are the unbound and the adsorbed state. Where the adsorption can be both chemisorption or physisorption. The unbound state is the sum of a chosen reference state of the adsorbate atom ( $E_{ref}$ ) and surface ( $E_{surf}$ ). The adsorption energies in this work are calculated according to Equation 2.24. In this work two reference states are discussed. Either with the adsorbate atoms taken as free floating individual atoms in a box, or bound as monolayers of material.

$$E_{ads} = E_{final} - (E_{surf} + E_{ref}). \quad (2.24)$$

With  $E_{ads}$  being the adsorption energy,  $E_{final}$  the energy of the system with the adsorbed atom,  $E_{surf}$  the energy of the surface without adsorbed atom and  $E_{ref}$  the reference energy of the adsorbed atom.

In the case of binding energy (where no surface is present) the equation turns into the following:

$$E_b = E_{bound} - x * E_{ref}. \quad (2.25)$$

Here  $E_b$  is the binding energy,  $E_{bound}$  the energy of the bound structure,  $x$  the amount of reference situations that are bound and  $E_{ref}$  the energy of the individual reference situation.

### 2.5.2. DFT calculations

All calculations were performed by DFT using VASP 5.4.4.[51],[52],[50]. The VASP program is widely available and easy to integrate in most systems. It is a plane-wave based code. The exchange correlation functional of Perdew-Burke-Ernzerhof (PBE) [78] was used for approximating the exchange-correlation energy. This has been a choice made after optimisation for the ruthenium bulk model. Later in the study (4.7) the vdW-DF2 functional is used as well. This is done to gain a better understanding of the vanderWaals forces present in the systems of bilayers. The interactions between valence electrons and ion cores is approximated using the Projector Augmented-Wave (PAW) method was used with a plane-wave basis set energy cutoff of 500 eV. In the calculations the partials occupancy's for orbitals are set in Fermi smearing. The width of smearing that is used is 0.2 eV. The energies obtained are considered converged when iterations resulted in differences of less than  $1 \times 10^{-7}$  eV. Iterations are considered converged when all atomic forces are below 0.001 eV/Å. In calculations where dispersion correction is taken into account the Grimme D3 scheme is used post-DFT [34], or the vdW-DF2 method is used [11], [25], [48]. For initial Ru(0001) surface optimisations a 1x1 7 layer symmetric slab with 25 Å vacuum is used on a k-point grid of 12x12x1. Afterwards a 4 layer asymmetric slab is used with a 15 Å vacuum starting at the bottom of the slab and a 12x12x1 k-point grid. All grids are from the Monkhorst-Pack. In coverage dependence calculations a 2x2 supercell is used formed from the asymmetric 4 layer slab. sub-monolayer coverage are simulated using 1 till 4 atoms (0.25 – 1ML). There the k-space is a 6x6x1 grid.

### 2.5.3. Bader charge analysis

To get an idea of the charge distribution over different atomic systems one can use the Bader charge implementation in VASP. The theory of Richard Bader is based upon the idea to bring molecular division back to charge density [5]. When there is no flux in the gradient field of the electron density, then the position can be described as the natural boundary of an atom. The Henkelman Group at the University of Texas at Austin has developed an implementation for this theory in the Vienna Ab initio Simulation Package (VASP) [88],[80], [39], [107]. The 2D surface for which the charge density is at a minimum perpendicular to the surface is what divides the atoms. The method of analysing charge is used to understand the charge transfer that might appear upon adsorption.



# 3

## Properties of ruthenium and phosphorus

### 3.1. Ruthenium

Ruthenium is a transition metal with atomic number  $Z = 44$  and as such is part of the iron-platinum group in the periodic table of elements. It has a hexagonal close packed structure with structure parameters,  $a = 2.71 \text{ \AA}$  and  $c = 4.28 \text{ \AA}$ [4]. The ABAB stacking and  $c$  and  $a$  values of the hexagonal close packed structure are shown in Figure 3.1. At room temperature it appears as a white or silver metal. Most notable uses for ruthenium are in the semiconductor industry, as catalyst, in medicine and for hardening of alloys.

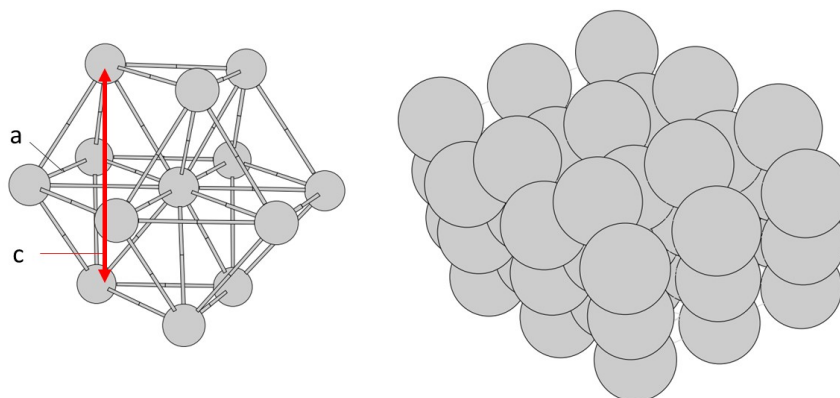


Figure 3.1: Hexagonal structure showing parameters  $a$  and  $c$  from [64]

### 3.2. Bulk Phosphorus

Phosphorus is the second element of the nitrogen group with atomic number  $Z = 15$  and a mass of 30.97 amu. It has a few stable allotropes, most notably white, red, violet and black phosphorus (Figure 3.2(a)-(d)). White phosphorus consisting of individual tetrahedral  $P_4$  molecules, where red phosphorus follows a chain-like structure and black phosphorus a sheet like structure. The most commonly found allotropes are white and red phosphorus [60],[58]. The allotrope of violet phosphorus can be formed heating red phosphorus in the absence of oxygen. Black phosphorus however is the most stable of allotropes [1],[61]. Phosphorous atom in its ground state has the electron configuration  $[\text{Ne}]3s^23p^3$ . As the  $3p$  subshell is half filled, the tendency to 'lose' or 'gain' electrons can roughly be estimated to be the same when in elemental form. Having 5 valence electrons, and thus one more than silicon, phosphorus is used as a donor dopant (n-type) in the semiconductor industry.

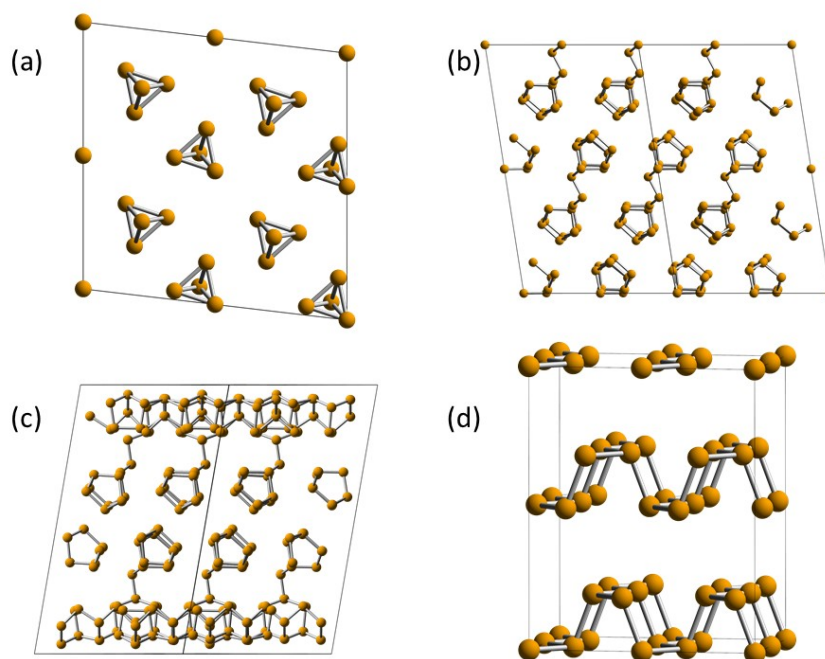


Figure 3.2: crystal structures of allotropes of phosphorus. (a) White phosphorus, (b) Red phosphorus (c) Violet phosphorus and (d) Black phosphorus. Images from Martin Uhrin [93]

### 3.3. Phosphorene

The emerging field of two-dimensional materials have led to some major breakthroughs in science over the last decades. Most notably the findings of Noselov, Geim and colleagues [73] on the properties of graphene. The "next big thing" in building electronic devices has lead the search for similar 2D materials with unique properties [13]. Phosphorene is one such materials of recent interest. The sheet-like structure has a corrugated profile, with a top view showing hexagons similar to graphene (Figure 3.3). It has a direct band-gap of 2 eV, and can be exfoliated from black phosphorus [16], [105]. Unlike graphene, phosphorene does not exhibit magnetic properties due to  $sp^3$  hybridisation bonding compared to  $sp^2$  hybridisation bonding [15] in graphene. The bond distances observed by Kulish and colleagues [53] are 2.22 Å and 2.26 Å for horizontal bonds and diagonal bonds respectively. The angle between horizontal bonds is 95.6 ° [103]. phosphorene tends to form bilayers which are reported to have bilayer distances of 3.09 Å using the optB86b-vdW functional and 3.50 Å using a PBE [78] functional [69].

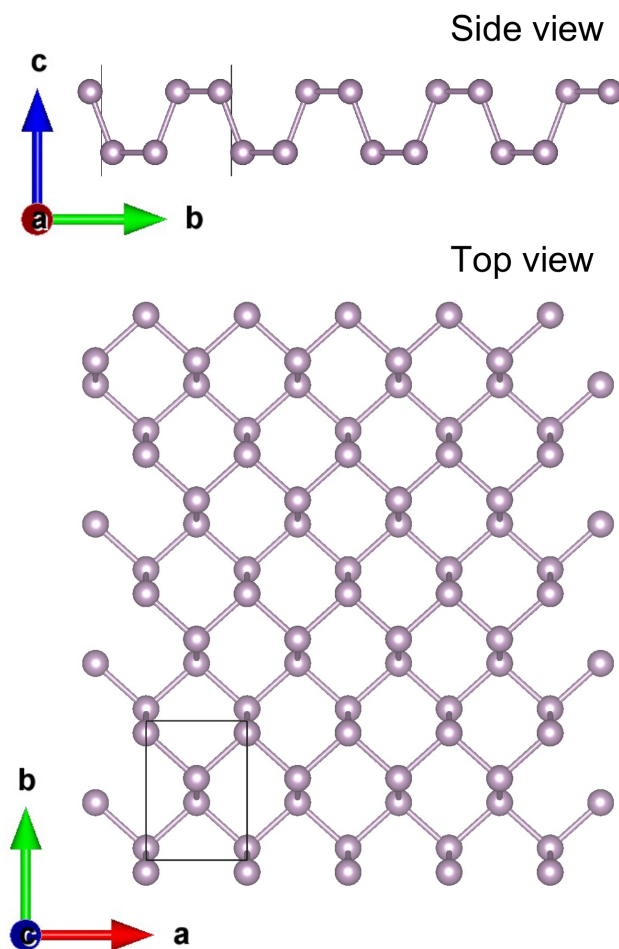


Figure 3.3: Side and top view of the two-dimensional (2d) phosphorene.

### 3.3.1. Phosphorene oxides

Multiple stoichiometries of phosphorus and oxygen are known to be stable. Both in the regimes of high P to O ratios [103] as well as low P to O ratios [68] [69] combinations are made. Structures close to that of phosphorene are reported (for  $P_4O_8$ ) showing corrugated sheets, but also ring like structures are found to be stable (for  $P_4O_2$ ). P-P bond lengths are increased slightly (2.32 and 2.37 Å for horizontal and diagonal) in phosphorene oxide. The x-y angle is increased to 100.9°.

### 3.3.2. Discussion and conclusion

Phosphorene is a two-dimensional material that could form from the rearranged adsorbed atoms on the surface. The corrugated structure visible in 3.3 makes it less likely to appear immediately since it would not have contact points all over the surface. The lengths of the horizontal bonds are close to those of the ruthenium bulk lattice (2.22 vs. 2.28 Å) however angles of 95.6° and 120° are not close and some strain would be needed to match the lattice (if the Ru bulk and surface lattice are close in size). Upon growth of layers of P, it would make sense if the P atoms would rearrange into corrugated sheets of phosphorene as weak bonds are needed to form between the layers. If O is present during adsorption of P on Ru(0001) and phosphorene oxide is formed, then the lattice mismatch with respect to Ru is reduced (100.9 vs. 120° and 2.32 vs. 2.28 Å). To model phosphorene through DFT one would ideally use a functional in DFT that accounts for vanderWaals interactions.

## 3.4. Phosphorus oxides

### 3.4.1. Phosphorus pentoxide ( $P_2O_5$ )

Phosphorus pentoxide, despite the name suggesting a  $PO_5$  stoichiometry, actually concerns a  $P_2O_5$  (diphosphorus pentoxide) structure. The crystalline phosphorus pentoxide has many uses in the chemical and medical world [29], [59]. It appears in different conformers of which the  $o'(P_2O_5)_\infty$  is the most common. D. Stachel[5] reported the structure of this  $o'(P_2O_5)_\infty$  to be constructed from layers of six-membered rings as seen in Figure 3.4 of three corner linked  $PO_4$  tetrahedra. The results are based on XRD experiments performed at 233 K. The phosphorus and oxygen atoms are described to have an average bond length of 1.570 Å for P-O bonds inside the rings and 1.440 Å for double-bonded oxygen atoms outside the ring. The unit cell (Figure 3.4) contains four  $P_2O_5$  units (28 atoms) and the crystallographic symmetry is orthorhombic with spacegroup Pnma. While the stability of the  $o'(P_2O_5)_\infty$  phase is long known, Arbib et. al. found that the  $o'(P_2O_5)$  phase is also orthorhombic with space group is Fdd2 but less stable using x-ray diffraction.[3] It is described to be made up from six-fold helices of  $PO_4$ -tetrahedra running parallel to the lattice  $c$ -axis. Each of these tetrahedra share three corners with adjacent helices, forming a three dimensional network as can be seen in Figure 3.4(d).

Structural, electronic and mechanical properties of two orthorhombic phases viz.,  $o'-P_2O_5_\infty$  and  $o-P_2O_5$  as reported in the literature [3, 83] are studied using DFT. [2]. They compared the previous experimental data with simulated optimal lattice parameters of the unit cell of the same compound using density functional theory (DFT) and found the simulations to agree very well to literature. Generalized gradient approximation based PBE exchange-correlation functional[78] is used. They also performed a few simulations using the local density approximation (LDA). The LDA based DFT calculations are found to deviate from reported experimental bond lengths by more than 2 percent if dispersion is not taken into account. The GGA based calculations proved to be more accurate, but still dispersion is needed to be accurate within 2 percent of experimental data. Including dispersion corrections improved structural description and the analysis of chemical bonding revealed mixed ionic and covalent character in both phases.

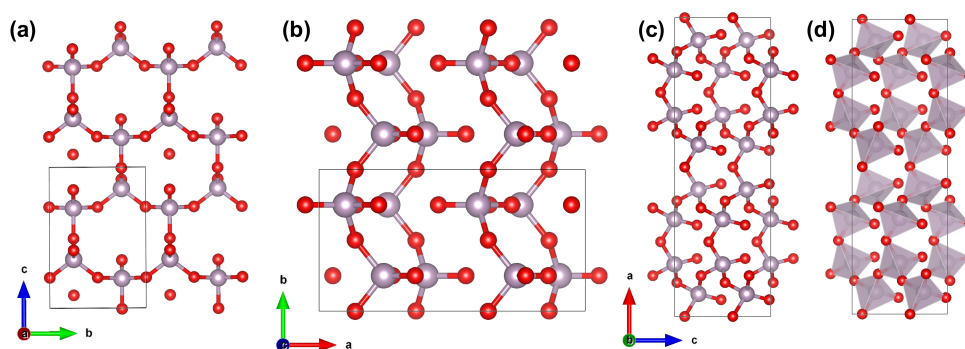


Figure 3.4: Computed unit cell of  $o'(P_2O_5)_\infty$ . Seen along the  $a$ ,  $c$  and  $b$  axis in (a), (b) and (c) respectively. (d) Shows the polyhedral projection.

### 3.4.2. Phosphorus trioxide ( $P_2O_3$ )

Compared to phosphorous pentoxide, a less common compound is phosphorus trioxide. Like pentoxide, its phrasing is misleading as it indicates one phosphorus atom where it has two per unit cell. The trioxide  $P_2O_3$  has a two to one ratio of doubly-bonded oxygen atoms to the single bonded ones. According to Van Wazer [95] phosphorus trioxide has a structure similar to that of phosphorus pentoxide with the exception that the four peripheral oxygen atoms are absent. The cage reported by Jansen and colleagues [43] can be seen in Figure 3.5. The P-O distances are reported to be 1.65 [38] [43] or 1.67 Å[72]. However this data is taken into account with the notion of its age.

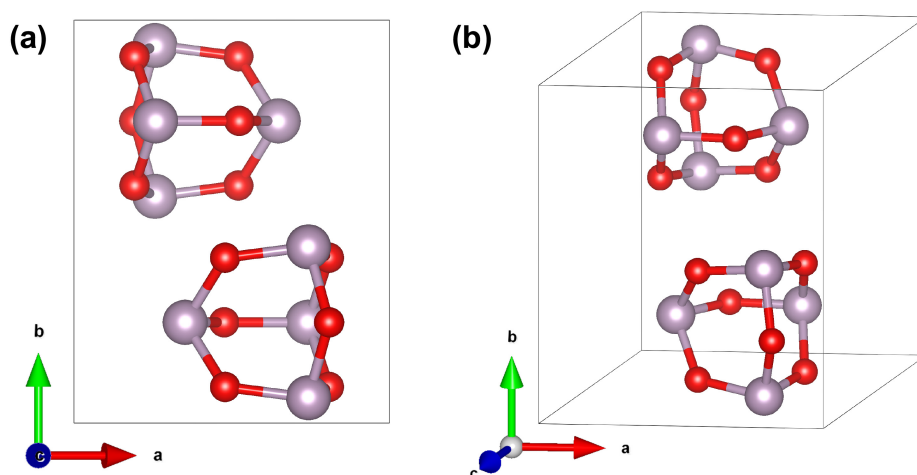


Figure 3.5: Computed unit cell of  $P_2O_3$  with the unit cell in (a) and the cage structure in shown in (b).

### 3.4.3. Discussion and conclusion

Of the phosphorus oxides the diphosphorus pentoxide is most stable and most likely to form on the Ru(0001) surface if enough P and O are present in the system. The bond lengths of any of the bonds in the oxides is smaller than the Ru lattice spacing (about 1.5 vs. 2.28 Å) this makes it unrealistic that any of the oxides grow directly from the surface onward. What can be deduced from the literature of phosphorus oxides is that to accurately model the interactions that these systems exhibit vanderWaals forces have to be taken into account and dispersion has to be modelled using DFT.

## 3.5. Ru(0001)-X, X = Si, O, S, N and C

After a thorough literature search, it could be stated that there are no studies, neither experimental not theoretical, concerning adsorption of phosphorous on a Ru(0001) surface. Therefore, adsorption of related elements in periods 2 and 3 of the periodic table of elements viz., Si, O, S, N and C on Ru(0001) are reviewed below in detail. The first paragraph of each subsection displays findings that consist of computational work, with the second section reporting experimental findings that are relevant to the study as well. The last element closely related to P is arsenic, however no relevant literature is found of adsorption of As on Ru(0001). Carbon in the form of graphene is included in the study as it is well studied and shows similarities to the graphene structure of Section 3.3.

### 3.5.1. Silicon/Silica

Löffler et al.[63] describe, using DFT, adhesion of a silica double layer to a Ru(0001) surface to be  $-32 \frac{meV}{\text{Å}^2}$ . Interactions between the silica sheet and transition metal surface are in the order of graphite-Ru(0001) interaction ( $-33 \frac{meV}{\text{Å}^2}$ ) with the main bonding coming from the dispersion term [63]. In a combined experimental and DFT study Chen et al. found that doping of Ru with Si causes the structure to change Si to fill the Ru threefold-hollow sites. This effectively weakens the adsorption of most atoms to the surface and can be exploited in HER [20]. Chang and Chou report from experimental work that having trace amounts of P contamination (1-2%) will promote the epitaxial growth of a metal-rich silicide [19].

### 3.5.2. Oxygen

Stampfl et al. [85] show that when oxygen comes in close contact with ruthenium the hcp hollow site as can be seen in Figure 3.6 is most favored for adsorption. The oxygen-ruthenium bond length is reported to be  $2.00 \pm 0.03$  Å. This is done using DFT with GGA and the PBE functional. The binding energy of O on the surface is 4.84 eV and 4.76 eV for the hcp and fcc site respectively [84]. During the adsorption of oxygen the first layer of ruthenium expands 3.7 % to 2.2 Å. In the report Stampfl et al. also compared to computational data with experimental Low Energy Electron Diffraction (LEED) to obtain similar Ru–O layer spacing and bond lengths.

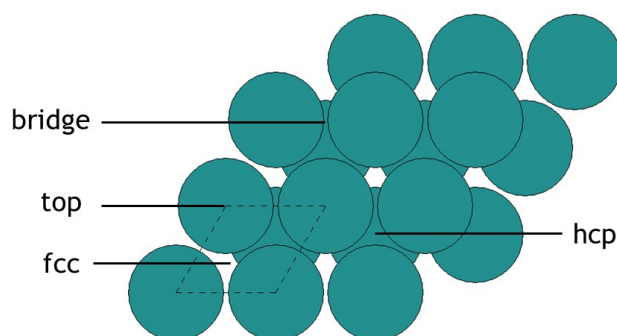


Figure 3.6: Ru sites shown schematically.

Molecular  $O_2$  on a clean Ru(0001) surface dissociates and forms a layer with a coverage of 0.5 ML according to Madey and colleagues [66]. The rate of oxidation is limited by the ruthenium sites as two are needed to dissociate an  $O_2$  dimer. Exposure after 1 ML will not follow this trend and instead the Ru(0001) surface will absorb dissolved atomic oxygen in the subsurface. This is however only the case at elevated temperatures.

For temperatures below 800 K Böttcher and Niehus do report through experimental data from Thermal Desorption Spectroscopy (TDS) and LEED that oxygen will penetrate to the subsurface when  $O_2$  molecules approach a full monolayer covered Ru(0001) surface. The behaviour will start appearing at 550 K if the Ru(0001) surface is in pristine condition. If however the Ru(0001) surface shows imperfections, the roughness is directly related to the onset of oxygen moving towards the subsurface at temperatures reported as low as 350 K [9]. Blume et. al. elaborated on this work further by stating that the oxygen will not go subsurface at temperatures below 500 K until the coverage reaches 2 monolayers. When the oxygen moves into the surface it will reside between the first and second Ru-layers effectively creating a meta-stable oxide locally [7]. When more than two monolayers of O are in the surface, then more O can adhere to the quasi-oxide saturating at 0.25 ML when 10 ML of O are in the subsurface [10]. Gsell and Menzel [35] reported that if the Ru(0001) surface is strained through the use of Ar gas bubbles, the location of tensile strain is the preferred place of adsorption for oxygen atoms. The suggestion is made that the lateral stress of the surface induced by the adsorption and stacking of oxygen on Ru(0001) lead to preference for areas where the strain is in tension compared to compression.

### 3.5.3. Sulphur

Atomic sulphur adsorbs on a Ru(0001) surface with binding energies of -5.76 eV and -5.66 eV for hcp and fcc respectively from DFT calculations [40]. The diffusion barrier from hcp to fcc is calculated to be 0.43 eV with the first one being the preferred site of adsorption. The sulphur will only occupy hcp sites for coverages below 1/3 ML from STM studies [41]. Schwennicke and colleagues reported that the S atoms do not occupy perfect hcp and fcc sites at full coverages, but instead are shifted by about 0.16 Å [81]. Changing the amount of sulphur adsorbing to a Ru(0001) surface, one can tune the electronic properties of the interface. The modified periodicity of the system and electron localisation on the monolayer of S causes an appearance of interface states in band gap of Ru(0001) [79]. This result stems from STM combined with DFT methods. Low energy electron diffraction (LEED) analysis shows a bond length of 2.28 Å whereas computational effort found a bond length of 2.35 Å seen in Figure 3.7 [40] using DACAPO [37], [32].

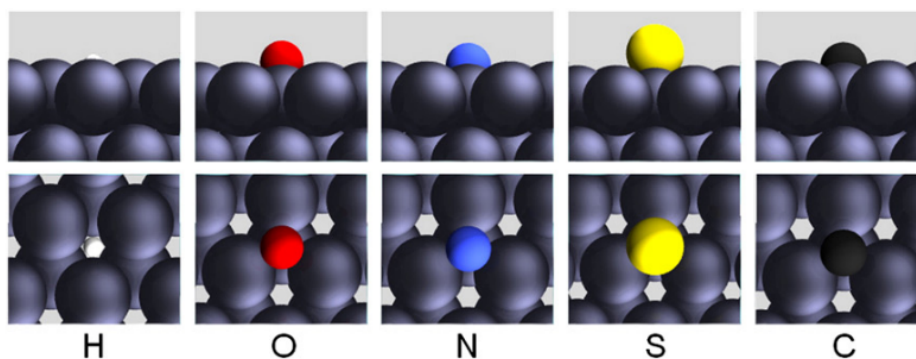


Figure 3.7: adsorbed atoms (H,O,N,S,C on a Ru(0001) surface from [40]

### 3.5.4. Nitrogen

Nitrogen, in elemental form, will adhere to the Ru(0001) surface with a binding energy of -5.46 eV and -4.92 eV, in the hcp and fcc sites respectively, when calculated using DFT/GGA [40]. Reported coverages of N on Ru(0001) are saturated at 0.38 ML [24] through desorption of  $\text{NH}_3$ . Herron et. al. reported the Dinitrogen adsorbed on Ru(0001) to have a binding energy of -0.24 eV in the hcp site and -0.74 eV in the top site [40]. LEED and DFT analysis estimate the nitrogen to be 1.05 Å and 1.11 Å above the surface respectively when bound in the hcp sites as can be seen in Figure 3.7 [40].

On the other hand, experiments show that Nitrogen in molecular dimer form does not readily adsorb to a Ru(0001) surface according to Danielson and colleagues [23]. Results are obtained using Auger Electron Spectroscopy (AES), LEED and Thermal Flash Desorption.

### 3.5.5. Carbon

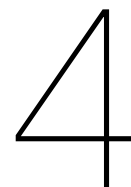
The adsorption of carbon in the form of graphene on Ru(0001) is studied more in depth both computationally ([100], [101], [46], [102], [70]) as well as experimentally ([97], [12],[87],[109],[30]). Wang and colleagues [100] show that corrugation of graphene sheets on Ru(0001) can be linked to buckling. The Ru(0001) surface bonds with the sheet stronger at some places leading to short Ru-C distances of 2.2 Å and weaker bonds between Ru and C resulting in distances of 3.7 Å at other places. A pattern resembling superstructures of h-BN is formed. The results have been found for both DFT using GGA as well as LDA type functionals. Jiang, Du and Dai [46] found the difference between lower and higher bound C atoms on Ru(0001) to be slightly higher at 1.7 Å. Both studies agree on the lowest C atoms to be 2.2 Å above the Ru(0001) surface. When a trilayer is present on the surface the graphene behaves as an isolated bilayer, LDA-based DFT simulations show that the decoupling is a result of passivation of metal d-states by the interfacial layer of graphene. Residual O in an oxidised layer of pure graphene will form crown ether rings where other cations can reside. These oxygen atoms have calculated binding energies of around 9 eV [36].

Experimental work of graphene on Ru(0001) also shows the formation of a "hump" in the graphene sheet using AFM combined with DFT at the GGA level [97]. Brugger and colleagues [12] mention that the graphene on Ru(0001) corrugated networks, like h-BN, are  $sp^2$  hybridized. This work has been done using angle resolved photo-emission (ARPES) experiments. Sutter and colleagues [87] also use ARPES and show that epitaxial graphene layers lose the corrugated structure when stacked on top of each other. The Dirac cones shown in isolated monolayers on the surface are recovered when there is a bilayer on the surface. When graphene is fully covering a Ru(0001) surface it becomes passivated to  $\text{O}_2$  adsorption at room temperatures. At elevated temperatures (>500 K) the oxygen will delaminate the graphene from the Ru(0001) surface through intercalation [109]. This is measured using STM, UPS and XPS. If graphene is doped with nitrogen on a Ru(0001) surface it will form a pyridinic N defect with a vacancy of C in it [30].

### 3.5.6. Discussion and conclusion

From the studies of O adsorption on Ru(0001) we can conclude that the O atoms adhere on hcp sites followed by fcc sites on the surface with Ru-O bonds lengths of around 2 Å and binding energies of around -4.8 eV. This is lower than the binding energies reported for S on the surface (around -5.7 eV)

but the preference of adhesion sites is the same. The S atoms being larger do not sit exactly in the sites. The S-Ru bond lengths are also larger than the O-Ru bonds (around 2.3 vs. 2 Å). Nitrogen binds with the same order of strength as the other related atoms, and shows a preference for the hcp site as well. From the studies on Si we can deduce that dispersion is of great influence on the binding mechanism on the Ru(0001) surface and should be taken into account if one performs DFT on the system with P. One can expect the phosphorus to bind in a similar fashion as reported for O and S, the binding of N would be of less relevance as the atom is of a significantly smaller size compared to P as can also be seen in Figure 3.7. If the surface of the Ru is strained, which one can expect on a surface and also from adsorption itself, the preferred place of adsorption is at the location of tensile strain. This could also mean that during the adsorption of P on Ru(0001) the P atoms could form a phosphorene layer which would strain the surface to match and adhere. The growth of O on Ru(0001) is reported to stop rather fast at intermediate temperatures (350 K) at 2 ML. The O atoms will move subsurface and reside between first and second layer of Ru. It is not expected to happen for P atoms as these are relatively large compared to O atoms. However one has to take into account that if the surface is rattling and defects are present, this would make it more likely. The study on Si revealed bilayers to form when O is also present, which is also happening if graphene is adsorbed on Ru(0001). The layers of graphene lose the "coned" structure of direct adhesion if more than one layer is adsorbed.



# Results and Discussion

## 4.1. Bulk phosphorous oxides

As can be found in the previous chapter, the two most stable oxide structures are phosphorus pentoxide ( $P_2O_5$ ) and phosphorus trioxide ( $P_2O_3$ ). Since they are the most common phosphorous oxide structures they are a good starting point for the calculations and subsequent model.

The study will focus on the comparison of a confined "bottom up" built small ( $< 10$  layers) structure of phosphorous (oxide) layer on a ruthenium surface. In order to find the mechanism in which phosphorus (and oxygen) will bind and grow on a ruthenium surface a number of steps have to be investigated. The first step would be to look at the bulk structures of phosphorous oxides that could possibly form. The initial setup of the computational model that is used can also be benchmarked against values from literature. Tables 4.1 and 4.3 summarise the results from the VASP DFT calculations. The PAW method was used with a plane-wave cutoff energy of 500 eV. To describe the XC-functional, the GGA based PBE functional was used.

The unit cell parameters are compared to experimentally found data to measure the setup of the computational system. To measure if the plane wave cutoff energy is sufficiently large to produce a representative value for the cell parameters a convergence test is done. Both the size of the reciprocal space as well as the energy of plane wave cutoff are tested for convergence. The structures for both  $P_2O_3$  and  $P_2O_5$  that are used as a starting point are retrieved from the materials project database [83], [65],[22],[44],[43].

Table 4.1: Unit cell lengths, volumes and total energy for phosphorus pentoxide  $P_2O_5$

K-space	Ecut [eV]	a [Å]	b [Å]	c [Å]	V [Å <sup>3</sup> ]	Etot [eV]
4x4x4	300	4.7353	7.0804	9.2496	310.12	-206.01
4x4x4	500	4.9400	7.3867	9.6496	352.12	-196.56
4x4x4	700	4.9375	7.3829	9.6447	351.58	-196.76
8x8x8	500	4.9400	7.3867	9.6497	352.12	-196.56
12x12x12	500	4.9400	7.3867	9.6496	352.12	-196.56
experimental		4.8904	7.1627	9.1939	332.05	

Table 4.2: Phosphorus pentoxide  $P_2O_5$  unit cell lengths and volume compared to Ainsworth et al. [2]

K-space	Ecut [eV]	a [Å]	$\Delta a$ [%]	b [Å]	$\Delta b$ [%]	c [Å]	$\Delta c$ [%]	V [Å <sup>3</sup> ]	$\Delta V$ [%]
4x4x4	300	4.735	-4.20	7.080	-3.82	9.250	-4.56	310.12	-12.07
4x4x4	500	4.940	-0.06	7.387	0.34	9.650	-0.44	352.12	-0.16
4x4x4	700	4.938	-0.11	7.383	0.28	9.645	-0.49	351.58	-0.32
4x4x4	900	4.941	-0.04	7.388	0.35	9.651	-0.42	352.30	-0.11
2x2x2	500	4.940	-0.06	7.386	0.33	9.649	-0.44	352.08	-0.18
8x8x8	500	4.940	-0.06	7.387	0.34	9.650	-0.44	352.12	-0.16
12x12x12	500	4.940	-0.06	7.387	0.34	9.650	-0.44	352.12	-0.16
2x2x2	952	4.943		7.362		9.692		352.70	

Earlier work done by Richard Ainsworth and colleagues showed that phosphorous pentoxide would form in a structure with unit cell parameters 4.943 by 7.362 by 9.692 Å. Table 4.2 shows that obtained values of modelled phosphorus pentoxide show excellent reproduction of the result from Ainsworth and colleagues. Using a plane wave cutoff energy of 500 eV and a 4x4x4 k-space the difference is between the obtained results and literature is negligible ( $< 0.5\%$ ) for all three unit cell lengths as well as the volume. The computational setup can be concluded to give correct estimates.

Table 4.3: Unit cell lengths, volumes, total energy and beta angle for phosphorus trioxide  $P_2O_3$ 

K-space	Ecut [eV]	a [Å]	b [Å]	c [Å]	V [Å <sup>3</sup> ]	Etot [eV]	angle $\beta$ [°]
4x4x4	300	8.108	6.720	6.863	336.1	-139.54	107.8
4x4x4	500	8.487	7.035	7.184	385.5	-133.51	107.8
4x4x4	700	8.483	7.031	7.181	384.9	-133.60	107.8
8x8x8	500	8.849	7.035	7.184	385.5	-133.51	107.9
12x12x12	500	8.487	7.034	7.184	385.5	-133.51	107.8
experimental		7.877	6.422	6.786	329.8	106.1	

As can be seen in Table 4.1 the cell parameters for phosphorous pentoxide are converged for values of 500 eV. The reciprocal space sampling a 4x4x4 Monkhorst-Pack grid is already converged. The values for the phosphorous trioxide show a similar trend in convergence visible in Table 4.3. There is however a discrepancy between the experimental results and the computationally obtained data. This is explained by the experimental data of the phosphorus trioxide. The experimental data of the phosphorus pentoxide are obtained from the work of Stachel and colleagues [83]. The experimental data of the phosphorus trioxide is retrieved from the work of M. Jansen et. al. [43]. The investigation of the structure by Jansen and colleagues can be considered outdated due to the time of publication. This alone however would not be enough argumentation to neglect the difference. There is also a fundamental difference in the unit cell that is taken from the structure. Where the experiment describes a structure with angle  $\beta = 106.1$ . the materials project file describes a rhombic prism unit cell with the same amount of oxygen and phosphorus atoms but different angles ( $\beta = 71.648$ ). With the angles adjusted the results do line up ( $\Delta = 1.5\%$ ). This is likely a result of the use of GGA based functionals in the calculations as these do not take into account the vanderWaals forces likely present.

Lastly we turn to the thermodynamic stability of the two phosphorous oxide phases. The atomisation energies as described in tables 4.4 and 4.5 show the energy difference there is between situation A where all atoms are treated separately and situation B where the atoms are bound in the phosphorus oxide structure.

Table 4.4: Atomization energies of phosphorus pentoxide  $P_2O_5$ 

K-space	Ecut [eV]	atomization energy per unit cell [eV]	atomization energy per atom [eV]
4x4x4	300	-159.520	-5.697
4x4x4	500	-149.976	-5.356
4x4x4	700	-150.173	-5.363
4x4x4	900	-150.210	-5.365
2x2x2	500	-149.867	-5.352
8x8x8	500	-149.976	-5.356
12x12x12	500	-149.976	-5.356

What is visible straight away is that the phosphorus pentoxide structure is more stable than the phosphorus trioxide structure as a whole. Also the atomisation energy per atom is lower. This means that if possible the phosphorus and oxygen atoms would most likely form a phosphorus pentoxide based structure given enough layers to display bulk behaviour. The values are however in the same order of magnitude and limitation in oxygen partial pressure could still influence the exact structure to form such as seen in work from Wang [104].

Table 4.5: Atomization energies of phosphorus trioxide  $P_2O_3$ 

K-space	Ecut [eV]	atomization energy per unit cell [eV]	atomization energy per atom [eV]
4x4x4	300	-105.588	-5.279
4x4x4	500	-99.557	-4.978
4x4x4	700	-99.654	-4.983
4x4x4	900	-99.671	-4.984
2x2x2	500	-99.558	-4.978
8x8x8	500	-99.557	-4.978
12x12x12	500	-99.557	-4.978

## 4.2. Ruthenium (0001) surface

The ruthenium surface as discussed throughout this work is an **hexagonal close packed (hcp)** 0001 surface which has ABAB stacking order. The x and y direction are in hexagonal structure. The optimised unit cell parameters of the ruthenium surface are 2.713 Å for the a and b parameters and 4.285 Å for the c axis. Here the angle between the a and b axis is 120°.

The surfaces of the X-ray mirrors used in ASML's lithography machines are covered by ruthenium and polished to atomic scale surface roughness. The ruthenium capping is generally polycrystalline. As a (first) starting point for DFT-based modeling it is approximated within periodic boundary conditions by a slab model that is based on the primitive (1x1) surface unit cell of the Ru(0001) surface. A small model will also give a good idea of the initial atomistic reactions that take place, while being computationally feasible within limited timescales. The energy of the system upon relaxation is taken as the unit of measurement for the convergence. The ruthenium slab as discussed above contains a seven layer symmetric surface with a combined 25 Å vacuum on both sides as can be seen in Figure 4.1(b).

Table 4.6: Final energy of a 7-layer Ru slab with different k-point sampling

system	k-space	E final [eV]
Ru	6x6x1	-62.679
Ru	8x8x1	-62.723
Ru	10x10x1	-62.657
Ru	12x12x1	-62.723
Ru	14x14x1	-62.684

Table 4.6 shows a k-point convergence test using a cut-off energy (Ecut) of 500 eV. there is not a very clear trend in convergence over k-space sampling grid size. Total energy convergence up to 50 meV is reached with 12x12x1 grid, which is why it is chosen for the subsequent calculations.

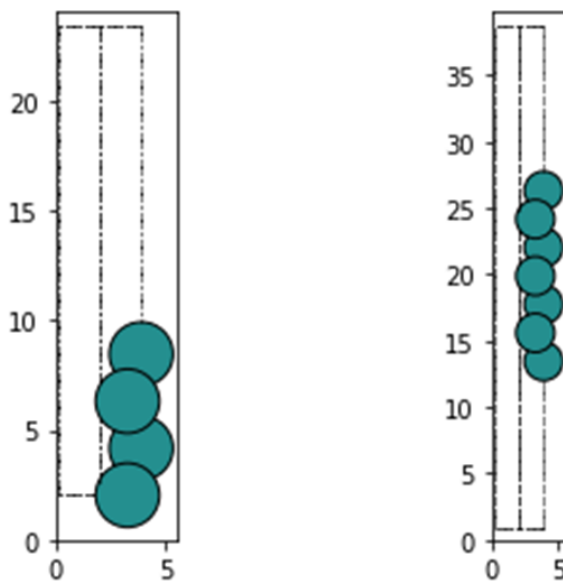


Figure 4.1: Slab models and 4-Layer asymmetric slab with 15 Å vacuum above the slab (a) and a 7-Layer symmetric slab surrounded by 12.5 Å vacuum on both sides (b)

#### Four Layer Asymmetric

In order to further reduce the computational effort, the size of the slab model is decreased to four layers and 15 Å vacuum. This is achieved by using an asymmetric surface which starts at the bottom of the calculated volume. When a symmetric slab is used, a four layer asymmetric surface slab as can be seen in Figure 4.1(a) is constructed with a total z-distance of at least 15 Å.

Table 4.7 compares how many layers of this asymmetric slab model have to be relaxed in order to get accurate surface behaviour. Three systems are compared, with either the top 2, 3 or all four layers relaxed. These geometry relaxations are performed both with only the PBE functional and PBE with applying a dispersion correction (PBE+D3). Since the D3 scheme [33],[34] only corrects geometrically and does not change the electronic states of the surface one can expect the same outcome of structure with tighter bonds and lower final energies using the dispersion correction.

Table 4.7: Final energies for 4-layer ruthenium surface after relaxing 2,3 or 4 layers.

layers relaxed	$E_{\text{final}}$ [eV]	PBE+D3
all	-34.918	-36.463
top 3	-34.919	-36.463
top 2	-34.895	-36.432

Table 4.7 shows as expected that tighter binding is found when using dispersion. It also shows that the system with the top 3 layers relaxed is a good estimate of full surface behaviour. The system where only two layers are allowed to relax differ more from the other two showing that the relaxation is not converged when only two layers are allowed to optimise positions. Therefore, in the following, only the bottom layer is kept frozen and the top 3 layers are being relaxed.

### 4.3. Geometric fit of phosphorous oxides on a Ru(0001) surface

After having established DFT models for bulk phosphorous oxides and the Ru(0001) surface, combining both to interfaces is a veritable both conceptual and computational challenge. Lattice mismatch and potential surface terminations need to be considered. The latter is helped by also considering insights about phosphorene structures, which have been in the focus of many recent studies in the context of two-dimensional materials.

Recent advances have been made in the discovery, production and study of two dimensional materials. There are multiple combinations of phosphorene and phosphorene oxides as mentioned in chapter 3.3. These all appear as stable sheet-like structures. As Malyi and colleagues showed in [68] oxygen and phosphorus form several stable two dimensional structures. A comparison is made between the overlap in area between the unit cells of these two dimensional structures and multiples of the primitive surface unit cell of the Ru(0001) surface in order to assess the commensurability of these structures. The Ru supercell sizes compared are  $1 \times 2$  till  $2 \times 6$ . The eight two dimensional structures are Phosphorene ( $P_4$ ) and phosphorene oxides ( $P_4O, P_4O_2, P_4O_6, P_4O_7, P_4O_8, P_4O_9, P_4O_{10}$ ). They can fit a certain amount of times in the area of a ruthenium supercell. If the area of the supercell in question is divided by the area of the two dimensional structures a first approximation can be made to see how many unit cells of the two dimensional phosphorene oxides will fit onto the supersurface. More importantly one can make an estimation of which structures would be more likely to form due to fit. The misfit between the two areas can give a preliminary idea which structures might form. If the strain is minimised, then the structures will likely not fit one to one, but the amount of effort needed will certainly be less compared to large misfit combinations. From these we can form a set of bar plots to show both the amount of phosphorene (oxide) area that will fit on the supersurface combinations, as well as the supersurfaces for which the area mismatch is small.

#### 4.3.1. Fit of 2D structures

The first comparison is made by measuring the area fit of phosphorene ( $P_4$ ) over the Ru(0001) supercells as can be seen in Figure 4.2. It is clear that a single unit area of phosphorene is smaller than the Ru(0001) unit area. The first bar of the  $1 \times 1$  unit area shows that the area of the surface is more than twice the area of the phosphorene surface. The bars shown in green have the smallest area misfit. When dividing the supercell areas over the phosphorene unit area, the resulting number is compared to the closest integer. If this difference is less than  $0.1 \left(\frac{\text{\AA}^2}{\text{\AA}^2}\right)$  the bar is colored green.

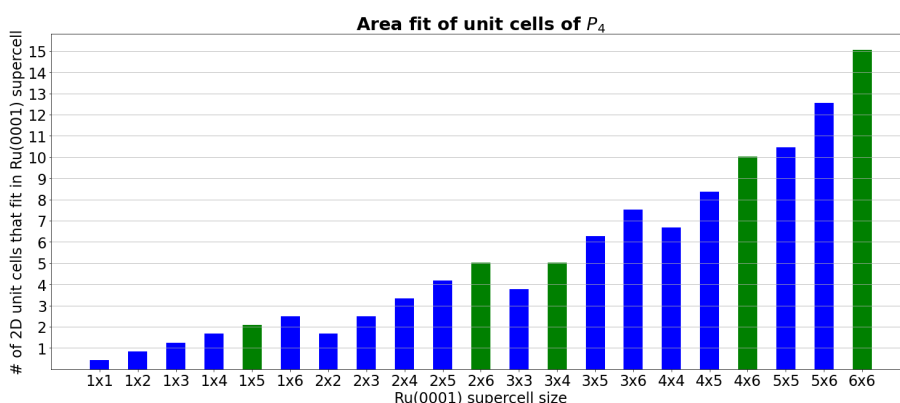


Figure 4.2: Area fit of a phosphorene ( $P_4$ ) unit area over different Ru(0001) supercell areas. Supercell combinations where rest strain to the closest integer (either compression or tension) is less than 10% of the unit area are denoted in green.

Of the 21 combinations of supercells four seem to be a close fit between the areas of phosphorene and the Ru(0001) surface. Since larger supercells are more expensive to calculate it makes sense to find an optimum of a representative system while maintaining as small as possible systems. In phosphorene the smallest system that would give a small misfit would be a  $1 \times 5$  supercell area. This is however an elongated cell that does not scale very well in both directions.

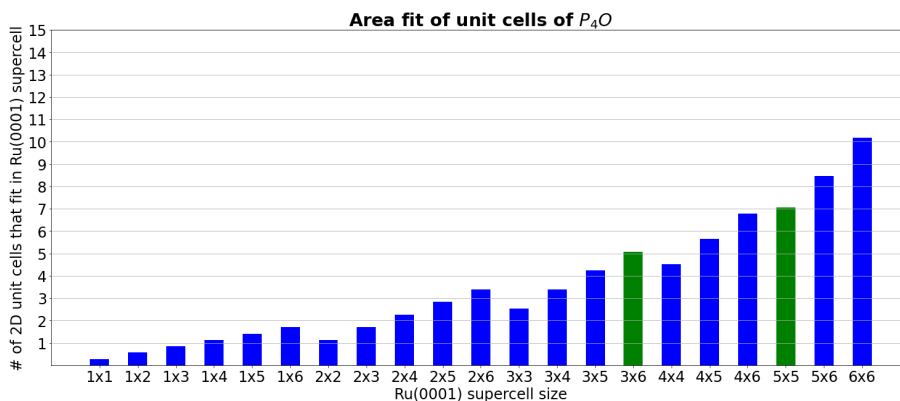


Figure 4.3: Area fit of a phosphorene ( $P_4O$ ) unit area over different Ru(0001) supercell areas. Supercell combinations where rest strain to the closest integer (either compression or tension) is less than 10% of the unit area are denoted in green.

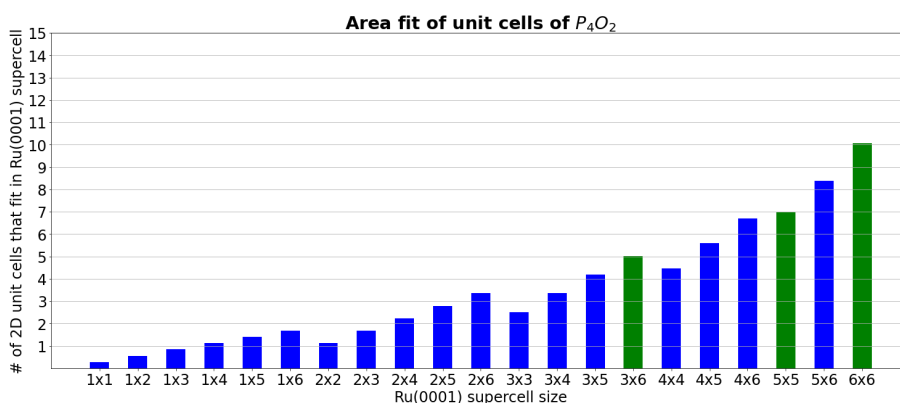


Figure 4.4: Area fit of a phosphorene ( $P_4O_2$ ) unit area over different Ru(0001) supercell areas. Supercell combinations where rest strain to the closest integer (either compression or tension) is less than 10% of the unit area are denoted in green.

As can be seen in Figures 4.3 and 4.4 the lower order phosphorene oxides differ in matching area to relatively small ( $< 3 \times 3$ ) supercells. This would make it more challenging to model them without either stretching the Ru(0001) surface or the phosphorene oxides in smaller systems. The larger order phosphorene oxides ( $P_4O_6$  till  $P_4O_{10}$ ) fit better in area to smaller supercells of the surface. This can be seen in Figure 4.5. There the  $2 \times 3$  supercell comes out as a possibly good fit to put the oxide on. This supercell size also is a good fit for the other higher order phosphorene oxides.

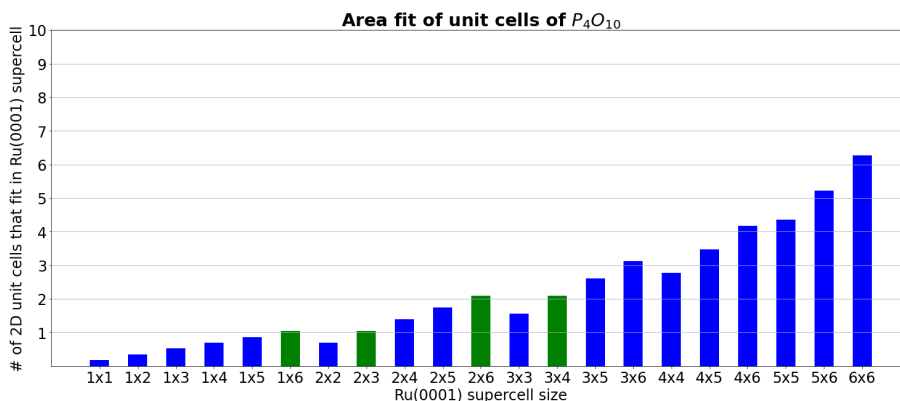


Figure 4.5: Area fit of a phosphorene ( $P_4O_{10}$ ) unit area over different Ru(0001) supercell areas. Supercell combinations where rest strain to the closest integer (either compression or tension) is less than 10% of the unit area are denoted in green.

From the study it is clear that for accurate modelling of phosphorene either an inconveniently stretched

supercell of 1x5 unit cells is needed or a 2x6 supercell. These are both computationally workable using DFT, however not within the timeframe of this project. Therefore it makes sense to approach modelling problem from the bottom up. One can model a small system and place individual atoms on and above the Ru surface to obtain relaxed structures within the lateral constraints of this model. This approach is studied in section 4.4.1.

## 4.4. Reference states of the adsorbate

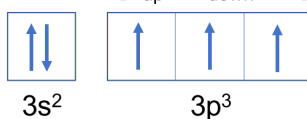
### 4.4.1. Atoms in a box

For the adsorption of P and O studied in the following section, the simplest reference of an adsorbate is to compare it to the energy of the atoms in a box multiplied by the amount of atoms present in the adsorbate. In reality it is not individual atoms that adsorb. It is more likely that some other forms of molecules or compounds in which the adsorbate is stable are present when it reaches the surface. For oxygen the most logical form is the diatomic allotrope. For phosphorus this can be tetragonal P<sub>4</sub> or for instance sheets or rings of black or red phosphorus respectively. Since the form in which the adsorbates appear on the surface is unknown at this point the initial study is being done using atoms in a box as comparison. Both phosphorus and oxygen can appear in different ground state configurations. Since phosphorus has 15 electron per atom, there are two different ways to fill the *p* subshell. All subshells from 1*s* till 3*s*<sup>2</sup> will be filled leaving three electrons left to divide over the 3*p*<sup>3</sup> subshell. In the quartet state all these electrons would be in the same up or down-spin. In the doublet state there would be one up-down pair and one unpaired electron. According to Hund's rule the all orbitals in a subshell must be half-filled before a single orbital can be completely filled. The quartet state, according to the rule, should be energetically favourable. This is verified for the DFT setup used here by a spin-polarized VASP calculation for a single atom in a large, asymmetric box of size 15 Å x 16 Å x 17 Å. As can be seen in Table 4.6 the ground state energy of the quartet state is ~ 6 times lower than the reported doublet state. From the combined data it is clear that the quartet state is more favourable and in this work can be taken as the state in which phosphorus atoms will be present.

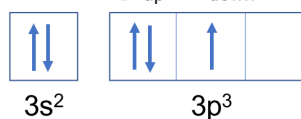
As for the oxygen, the same test has been done previously in the group to verify the triplet state to be lowest in energy. This was confirmed to be the lowest energy state. In the report the assumptions of the quartet state ground state for phosphorus and the triplet ground state for the oxygen atoms are used in any energy-based results.

#### Phosphorous (P)

Quartet [ $n_{\text{up}} - n_{\text{down}} = 3$ ]

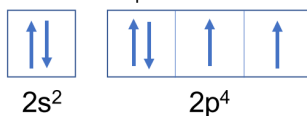


Doublet [ $n_{\text{up}} - n_{\text{down}} = 1$ ]

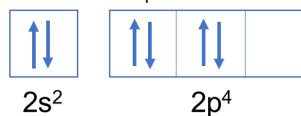


#### Oxygen (O)

Triplet [ $n_{\text{up}} - n_{\text{down}} = 2$ ]



Singlet [ $n_{\text{up}} - n_{\text{down}} = 0$ ]



$n_{\text{up}}$  – no. of spin-up electrons

$n_{\text{down}}$  – no. of spin-down electrons

Figure 4.6: Different electronic configurations for phosphorus and oxygen considered here. The respective ground states (according to Hund's rule) are shown on the left, and an electronically excited state is shown on the right.

Table 4.8: Ground state energy of phosphorus in electron volts

	ground state energy [eV]
doublet	-0.3169
quartet	-1.8721

Using the stated ground state configurations total energies are calculated as a function of cut off energy of the plane waves in the computational setup. Since more computational cost is needed for a higher plane wave cut off energy it is key to use a correct energy for both producing representative results as well as saving computational cost. In table 4.9 it becomes clear that for these simulations the computational cost for a good estimate is low. At cut off energies of 400 eV the value of the single phosphorus atoms is converged. This is not the case for the oxygen atom seen in table 4.10. There the value of 400 eV would not be sufficient. The value of 500 eV however differs 1 meV from the result of 700 eV and can therefore be considered converged. This trend is in line with previous simulations from table 4.2 where a cut off energy of 500 eV will yield results that are within the margin of error for the DFT setup used at the time of writing.

Table 4.9: Ground state energy of single atom of phosphorus

element	$E_{cut}$ [eV]	total energy [eV]
P	400	-1.876
P	500	-1.876
P	600	-1.876
P	700	-1.876

Table 4.10: Ground state energy of single atom of oxygen

element	$E_{cut}$ [eV]	total energy [eV]
O	400	-1.565
O	500	-1.579
O	600	-1.578
O	700	-1.578

#### 4.4.2. Free-standing phosphorus monolayers

Later on in the study the chosen reference is made using monolayers of phosphorus. Unlike oxygen, phosphorus does tend to bind in an ordered manner and can form sheet like structures. When dealing with a small cell with periodic boundary conditions it makes sense to model the reference adsorbate as a sheet, the same way the surface is modelled. Using monolayers of phosphorus as reference state takes chemical binding within the layer (and concomitant overlap of electronic orbitals) already into account and thus allows to focus on the binding to the Ru(0001) surface. The lateral binding inside the phosphorus layers does indeed lead to pairing of electrons, as illustrated by Figure 4.7. Here the total energy as a function of unpaired electrons is shown, which can be fractional in the DFT formalism. Unlike for the P atom in a box discussed in the previous section, for the phosphorus layer, the lowest energy is obtained with zero unpaired electrons, which corresponds to a non-spin-polarized calculation. Changing the reference will shift the outcome of energies, but does not change the difference between the systems measured.

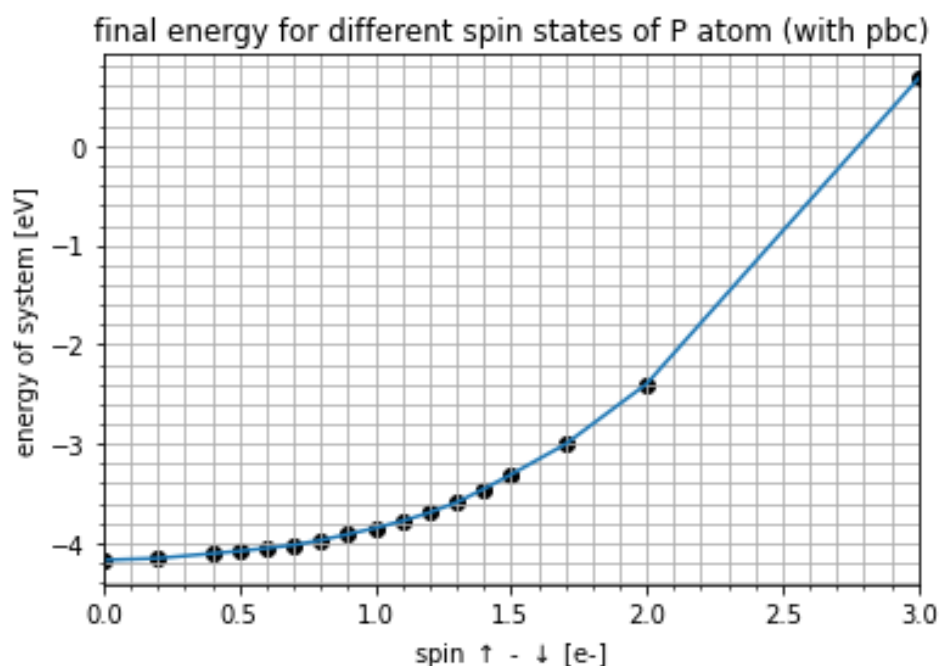


Figure 4.7: Final energy of a P monolayer plotted for different spin states

## 4.5. Monolayer adsorption

Following the bottom-up approach for studying the layer-by-layer build-up of phosphorus (oxides) on the Ru(0001) obviously starts with studying the adsorption of a single monolayer. The main focus of this section is therefore to answer the following questions: what are the most favorable adsorption site and concomitant adsorption energy for a monolayer of oxygen and phosphorus on Ru(0001), henceforth defined as one adsorbate atom per surface atom?

the ruthenium(0001) surface contains four high-symmetry sites which imply the highest possible metal-adsorbate coordination and thus are most likely adsorption sites as can be seen in Figure 3.6. The hcp hollow site is in the valley between the three ruthenium atoms directly above the ruthenium atom two layers below. The adsorbate will fit into ABAB sequence of the ruthenium layer. The fcc site is in a similar valley as the hcp site, but with the difference that it does not lay exactly above a ruthenium atom and thus will not be following the ruthenium stacking sequence. The bridge site is in between two atoms. The last high-symmetry site, with lowest coordination, is simply on top of the surface atom. For the DFT calculation, P and O atoms are initially placed in close proximity to the surface at a distance of 2 or 1.27 Å for P and O respectively. The starting points are varied by placing the adsorbate atom above the four high coordination sites, or above the surface in a position that is laterally between high coordination sites. Initially the adsorbate atoms are fixed laterally to check the differences between the distinct sites. During the next iteration the atoms are relaxed in all directions to verify if the high coordination points are indeed local minima of the potential energy surface. The values of adsorption energies are calculated according to section 2.5.

Table 4.11: Adsorption energies of phosphorus on 4 high coordination sites in eV

	PBE	PBE+D3
hcp	-4.433	-4.730
fcc	-4.310	-4.603
bridge	-4.124	-4.401
top	-3.862	-4.192

Table 4.12: Adsorption energies of oxygen on 4 high coordination sites in eV

	PBE	PBE+D3
hcp	-5.416	-5.486
fcc	-5.267	-5.326
bridge	-4.401	-4.455
top	-4.293	-4.425

The four positions are indeed local and in the case of hcp the global minima of the potential surface. All adsorbate atoms given the chance move laterally to one of the four high coordination sites. As can be seen in Table 4.11 and 4.12 the most favourable site for both oxygen and phosphorus to adsorb is the hcp-hollow site. The second strongest adsorption is found for atoms on the fcc site followed by the bridge and the top site. For equivalent sites, oxygen is bound more strongly compared to the phosphorus.

### 4.5.1. Coverage

So far, only a 1x1 surface unit cell has been used. This does not allow to model coverage lower than a full monolayer, since all laterally translated "copies" of the high-symmetry adsorption sites are equivalent for this choice of periodic boundary conditions. Repulsive lateral interactions between adsorbate atoms are likely to make lower coverages more energetically favorable. The P coverages, ranging from  $\theta = 0.25$  ML till  $\theta = 1$  ML are shown in Figure: 4.8,4.9,4.10,4.11. This coverage dependence of adsorption of oxygen and phosphorus on a ruthenium surface is shown in the Table 4.13 and Figure 4.12.

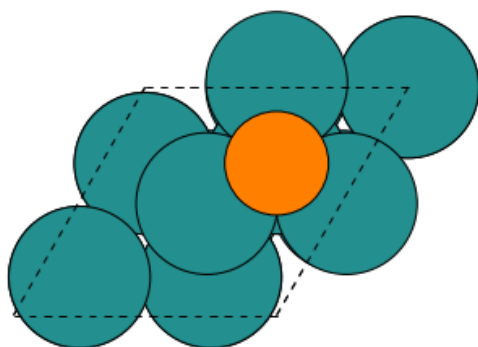


Figure 4.8: Top view of 2x2 cell with a single Patom on an hcp site on the Ru(0001) surface. This corresponds to  $\theta = 0.25$  ML

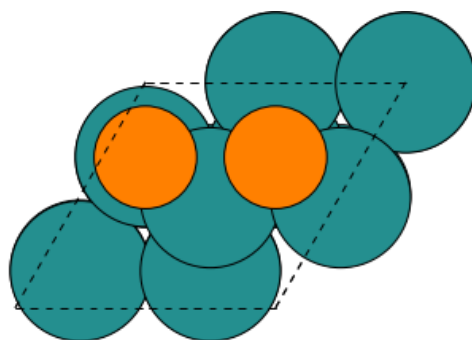


Figure 4.9: Top view of 2x2 cell with two Patoms on an hcp site on the Ru(0001) surface. This corresponds to  $\theta = 0.5$  ML

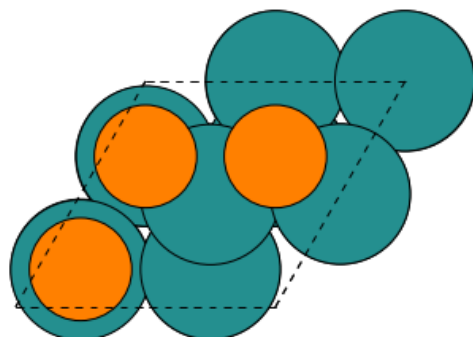


Figure 4.10: Top view of 2x2 cell with a three Patoms on an hcp site on the Ru(0001) surface. This corresponds to  $\theta = 0.75$  ML

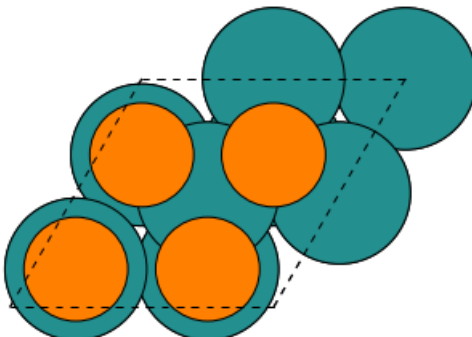


Figure 4.11: Top view of 2x2 cell with four Patoms in on hcp site on the Ru(0001) surface. This corresponds to  $\theta = 1$  ML

Table 4.13: Coverage dependence of adsorption for phosphorus and oxygen atoms on a ruthenium surface

$E_{ads}/atom$ [eV]	P	O
0.25ML	-5.466	-5.973
0.5ML	-5.136	-5.651
0.75ML	-4.860	-5.411
1ML	-4.545	-5.163

The coverage dependence study is made using a 2x2 unit cell containing a four layer ruthenium surface. Table 4.13 that for lower coverage, the adsorption energy per atom decreases (the adsorption energy  $E_{ads}$  lowers), i.e. the binding becomes more energetically favorable. The linear trend between the coverage and adsorption energy, as illustrated by comparing the slopes of the different lines, is very close for both oxygen and phosphorus. The coverages have similar slopes (1.07 (O) and 1.22 (P) eV/ML) as can be seen in Figure 4.12. All adsorption energies were in the same order of magnitude ranging from -4.545 (P  $\theta = 1$ ML) till -5.973 (O  $\theta = 0.25$  ML) eV. This means that while adsorption is stronger when the coverage is below 1 ML, the 1 ML 1x1 setup will still be an accurate way of learning about positional preferences and growing methods.

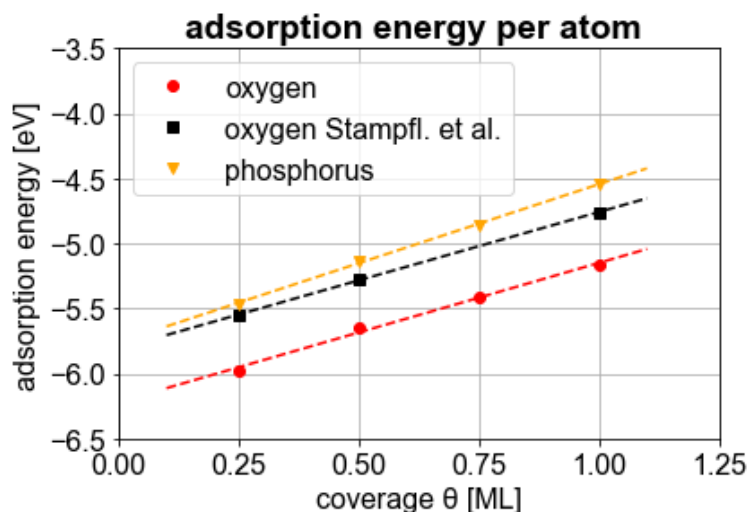


Figure 4.12: Coverage dependence on a ruthenium surface

The values for oxygen can be compared to literature. Work by Stampfl and Scheffler [85] showed a similar trend in coverage dependence for oxygen on Ru(0001) as can be seen in Table 4.14. There is a difference of about 7 to 8% between the obtained adsorption energies and the values from the work of Stampfl. and colleagues.

Table 4.14: Coverage dependence compared to Stampfl. et al. [85]

	$E_{ads}/atom$ [eV]	Stampfl. et al.	% difference
0.25ML	-5.973	-5.55	7.6
0.5ML	-5.651	-5.28	7.0
0.75ML	-5.411	ND	
1ML	-5.163	-4.84	8.5

Though the exact numbers differ by around 300 meV between the calculations of Stampfl et al. and our results, one thing is clear. The slope of coverage dependence is nearly identical (1.5% difference) for both systems as can be seen in Figure 4.12. The differences are due to improvements in the accuracy of the plane-wave DFT setup used in the present compared to those about 25 year-old calculations, most likely regarding the reference state of atomic oxygen.

## 4.6. Multilayer adsorption

Extending the work of the previous section 4.5 is essential in order to gain further insights in growth from the atomistic scale. Focusing on the for high-symmetry sites for the adsorption of the P and O atoms that form the second layer gives four times four sites totalling to sixteen discrete combinations. To properly estimate the difference between these combinations the lateral directions are constrained initially in the geometry optimizations. This will cause the atom to only be able to move in the vertical direction and thus stay in the high coordination site.

### 4.6.1. Two layers

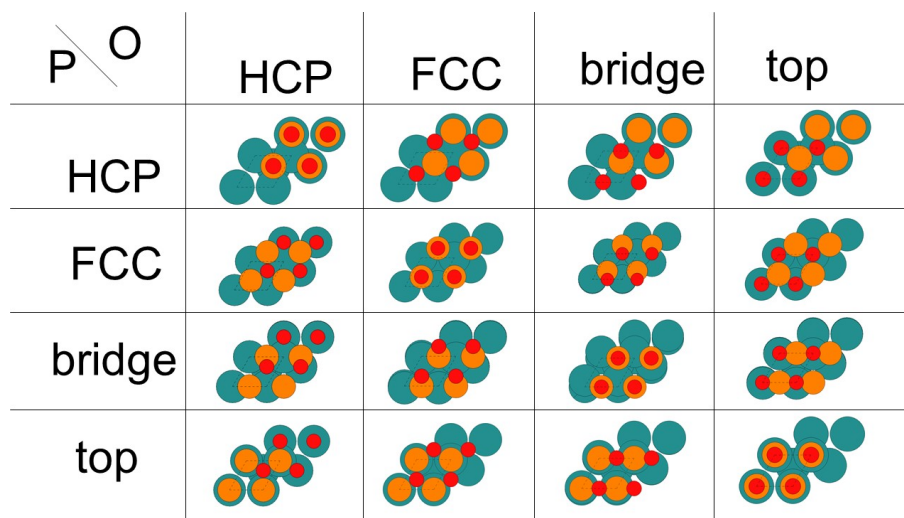


Figure 4.13: 16 High coordination site positions with an oxygen atom above a phosphorus atom above the Ru(0001) surface. The ruthenium atoms are shown in green, the phosphorus in orange and the oxygen atoms in red.

In Figure 4.13 the 16 different combinations are depicted schematically. The names of the positions are always relative to the the Ru(0001) surface. The combination hcp-top will follow the Ru(0001) stacking order. The initial distance between the topmost ruthenium atom and the phosphorus atom is 2 Å, the initial distance between the phosphorus atom and the oxygen atom is 1.27 Å.

Table 4.15: Adsorption energies per atom for 16 combinations of 2 atoms in 4 high coordination sites in eV

1st atom \ 2nd atom	O hcp	O fcc	O bridge	O top
P hcp	-2.210	-4.643	-4.599	-4.220
P fcc	-4.632	-2.157	-4.577	-4.197
P bridge	-4.435	-4.399	-2.056	-4.113
P top	-4.077	-4.047	-4.212	-1.867

In table 4.15 there is a clear trend for combinations which are favored over others. The combination of one atom in a hcp-hollow position and the second atom in the fcc position gives the strongest adsorption. If the phosphorus atoms closest to the surface (1st atom) is in the hcp position, the adsorption energy is at its lowest of the set. The strongest adsorption is found to be -4.643 eV with reference to atoms in a box. In Table 4.16 the same trend of preferred combinations is found when dispersion is included in the simulation. The binding is stronger due to the contribution of vanderWaals forces.

Table 4.16: Adsorption energies per atom for 16 combinations of 2 atoms in 4 high coordination sites in eV including dispersion

1st atom \ 2nd atom	O hcp	O fcc	O bridge	O top
P hcp	-2.406	-4.897	-4.852	-4.471
P fcc	-4.886	-2.352	-4.773	-4.447
P bridge	-4.698	-4.650	-2.253	-4.359
P top	-4.312	-4.280	-4.443	-2.054

The previous results of table 4.15 and 4.16 are assuming the phosphorus atom to always be the first atom on the ruthenium surface. This is of course not automatically the case. Next we compare the results to the set where the oxygen atom is the first atom on the surface and the phosphorus atom is in a position above it. The first notice is the fact that for almost every combination the situation of oxygen closest to the surface will result in weaker adsorption. The strongest adsorption for a Ru–O–P combination (visible in 4.14) is found when both oxygen and phosphorus adsorb on the bridge site. However this position still gives less adsorption energy per atom than ten of the sixteen combinations using a Ru–P–O stacking. In Figure 4.14 The final combinations are visible. The resulting adsorption energies are tabulated in table 4.17. Unlike the systems of O above P on Ru(0001), not all combinations yield adsorption in the first place. In Table 4.17 it is visible that P in the fcc site above O in the bridge site, as well as all combinations where O is on top of the Ru surface (except for O on top, P on bridge) show repulsion. In Figure 4.14 it is also visible that all combinations where the oxygen atom is on top of a Ru atom in the initial position, the adsorbate atoms will switch places and oxygen will end up above the P.

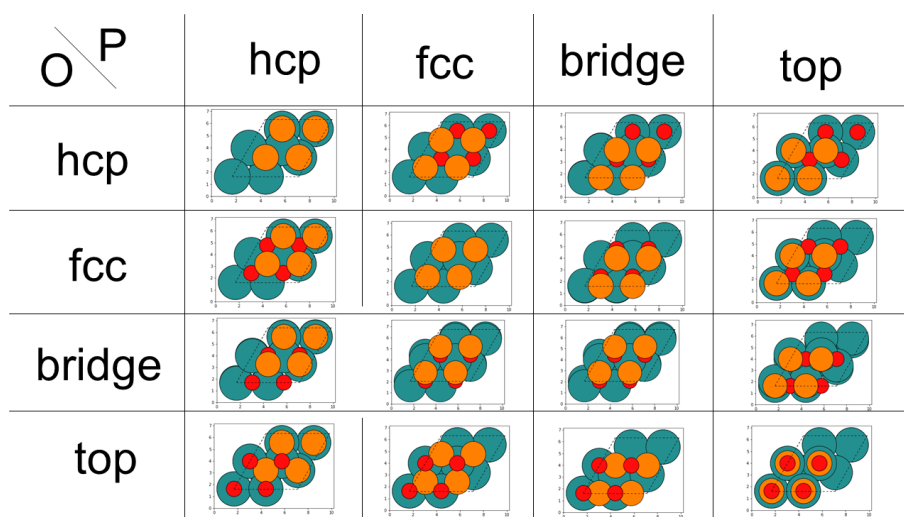


Figure 4.14: 16 High coordination site positions with a phosphorus atom above an oxygen atom above the Ru(0001) surface, the ruthenium atoms are shown in green, the phosphorus in orange and the oxygen atoms in red.

Table 4.17: Adsorption energies per atom for 16 combinations of one phosphorus atom on one oxygen atom in 4 high coordination sites in eV

1st atom \ 2nd atom	P hcp	P fcc	P bridge	P top
O hcp	-3.823	-3.887	-3.772	-3.887
O fcc	-3.871	-4.314	-3.771	-3.871
O bridge	-4.021	32.289	-4.327	-3.506
O top	8.280	8.280	-3.510	8.127

For continuing further towards modeling multi-layer formation, it is important to know how the atoms behave when the lateral constraints are lifted. A logical next step is thus to take the favourable combinations and remove the lateral constraints. The (1x1) model does provide the freedom to move to a more favourable position that would be a "trade-off" between the sites. This is verified by restarting

from the combinations with most favorable adsorption energies, releasing all lateral constraints. Table 4.18 shows the values of adsorption with and without lateral constraints and the percentage of change between these two. Two combinations show a change in final position (and thus adsorption) upon lateral relaxation. When there is a surface with on it an O atom and above that a P atom in bridge and hcp site respectively the largest change (7.7%) is observed. The other change is found when the positions are the same but the elements are switched. Then the Ru(0001) surface is stacked with P in hcp and O in bridge site above. This combination gave a 1.3% stronger adsorption when lateral constraints are released. All other combinations show the exact same optimal position.

Table 4.18: Adsorption energies per atom for combinations of 2 atoms in 4 high coordination sites in eV using P and O atoms, without lateral constraints.

1st adsorbate	2nd adsorbate	constrained	not constrained	% stronger adsorbed
O-bridge	P-bridge	-4.327	-4.329	0
O-bridge	P-hcp	-4.021	-4.329	7.7
O-fcc	P-fcc	-4.314	-4.314	0
P-fcc	O-bridge	-4.577	-4.577	0
P-fcc	O-hcp	-4.632	-4.632	0
P-hcp	O-bridge	-4.599	-4.657	1.3
P-hcp	O-fcc	-4.643	-4.643	0

Since most of the combinations using two atoms show stronger adsorption when phosphorus is the atom closest to the ruthenium surface. Also the adsorption of phosphorus on a phosphorus layer is being considered (Ru–P–P).

Table 4.19: Adsorption energies per atom for 16 combinations of 2 atoms in 4 high coordination sites in eV using 2 phosphorus atoms.

1st atom\second atom	P hcp	P fcc	P bridge	P top
P hcp	-3.580	-3.552	-3.731	-3.370
P fcc	-3.537	-2.912	-3.205	-3.332
P bridge	-3.244	-3.273	-3.347	-3.313
P top	-3.200	-3.157	-3.133	-3.412

Compared to Tables 4.15 and 4.17 using two phosphorus atoms results in weaker adsorption overall compared to a stacking using phosphorus and oxygen. Adsorption is stable for all of these combinations ( $E_{ads} < 0$ ). The difference in adsorption strength that is found between the weakest and strongest adsorbing combinations is less than 0.6 eV indicating a flattening of the potential energy surface (PES). This can be explained by the difference in radius of the outer electron shells of oxygen and phosphorus. With the latter having a higher radius and can therefore not be as close to the surface as the smaller atom (O) can. The difference can also be the reasoning for the stronger adsorption of O atoms in the first layer results of section 4.5.

#### 4.6.2. Three and more layers

When adding the third atom in a P–O–P hcp-bridge-hcp combination on top of the Ru(0001) surface, the third atom or highest P atom will tend to hover in a position about 3 Å above the adsorbed bilayer. Indicating that it is not likely to form as a trilayer. Since the final energy of this system still shows adhesion of all atoms a check is done to plot the potential of the the third phosphorus atom and its distance to the adsorbed bilayer shown in Figure 4.15. The 1-D potential plot should ideally show a short range repulsion part where the atoms are too close and outer shells would overlap and interfere leading to a repulsive force and thus a higher total energy. Next to this part should be a well in which there is an optimum distance for the third atom to sit and bind to the bilayer. The last part of the plot should show a weak long-range interaction in which binding would still be happening but with decreasing strength over longer distances.

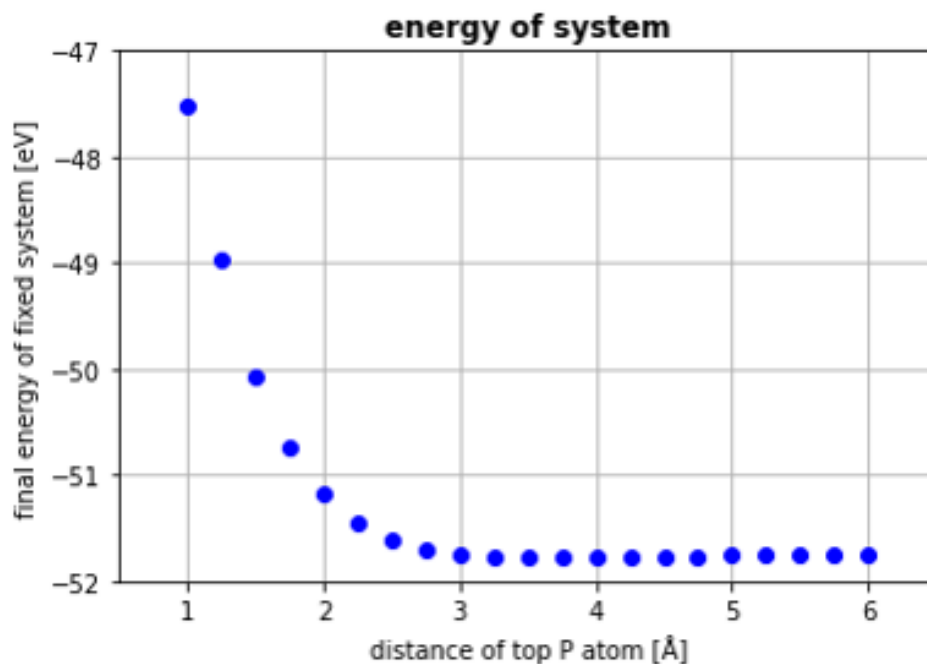


Figure 4.15: Final energy of system in VASP plotted against distance of third adsorbate atom above the second one in the situation of Ru-P-O-P.

When looking at Figure 4.15 it becomes clear that although the short range repulsion is there, the other two parts of the expected potential curve are not present. Upon closer inspection there is a minimum, however the difference is in the meV range and is thus smaller than computational accuracy. The right hand side of the Figure also shows that although distance is increasing for the topmost atom, the energy does not change. This would indicate that the distance of that atom does not have any effect on system. This is strange from a physical point of view, since the optimum bonding distance will likely not be kilometers away. As it is not likely to form, the study is moved towards the adsorption of layers of P on the surface.

### Charge transfer

The Bader charges, see section 2.5.3, reveal that throughout the simulation with the three adsorbates P-O-P in hcp-bridge-hcp there is charge transfer from the bottom P atom and the O atom. Where the outer shells in the initial setup measure 6 and 5 electrons for O and P respectively, in the end this turns to 8 and 3. By having 8 electrons in its outer shell one can expect the oxygen to behave noble. The filling of the outer shell will decrease the electronic affinity that drives bonding. This is a possible explanation of the repulsion of the third adsorbate above the oxygen atom. Interfacial charge transfer effects from thin layered black phosphorus to metal nano-particles was found and described by Peng et al. [77]. The charge transfer is analysed for the system of only P on the surface. Here charge transfer effects are negligible as can be seen in Figure 4.16. There is a small amount of charge transfer visible at the interface in the order of 0.1 e-. Here there seems to be a small charge accumulation from the Ru(0001) surface and the second adsorbate layer. Any higher layers show virtually no charge transfer. The growth can therefore be assumed not passivizing through charge transfer. This rules out the model of Cabrera and Mott to govern the way how P is stacked on a Ru(0001) surface. There is no passivation present, through the limiting transfer of charge.

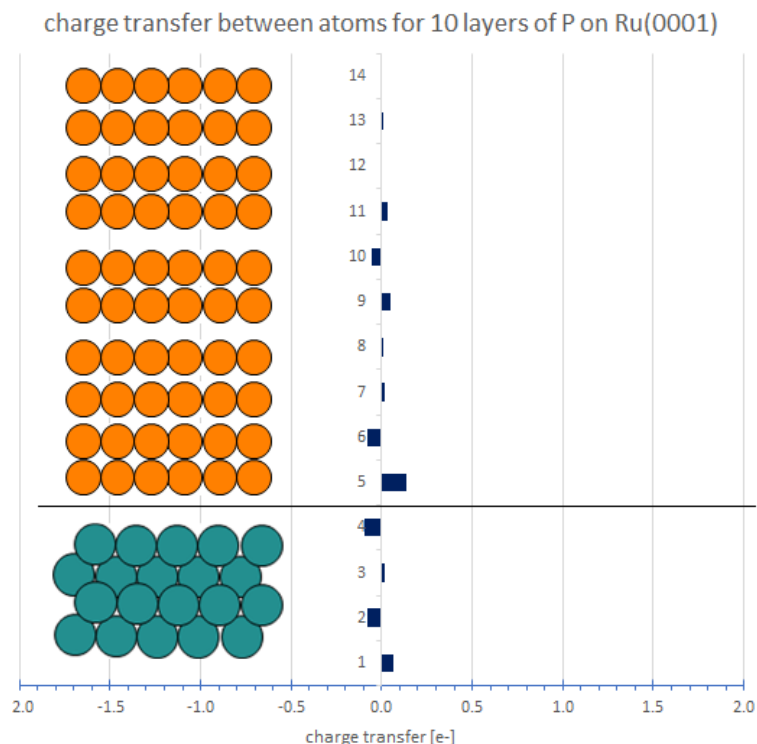


Figure 4.16: Charge transfer between layers in a system of 10 layers of P on top of Ru(0001) [e-]

### 4.6.3. Energetics

To look at adsorption of multiple layers of P on the surface a set of simulations is done with increasing number of P adsorbate atoms. The first atom on top of the surface is placed 2 Å above the Ru(0001) surface. From there every next atom is placed 2.18 Å above the previous one. This process is repeated till 14 phosphorus atoms are directly above each other. Every one of the systems ranging from 0 adsorbed till 14 adsorbates is relaxed in with a 50 Å vertical vacuum. The results are shown in Figure 4.17 and describe the layer by layer behaviour of phosphorus on the Ru(0001) surface.

All atoms are positioned in the hcp-site in reference to the Ru(0001) surface. According to the Cabrera-Mott theory, at a number of layers the adsorption energy will turn positive and the layer will adsorb no more atoms. What happens does not follow this trend. When adsorbing more and more atoms the adsorption energy per atoms starts to plateau. The adsorption energy is still negative at -1 eV, but does not change anymore between atoms added. Instead of passivation behaviour, the adsorbate approached bulk-like behaviour. This trend is visible for all functional approaches. The PBE functional (blue line) shows values in between the vdW-DF2 functional and PBE+D3 (orange curve) functional. The latter one showing overbinding compared to the other two, leading to lower adsorption energies. The vdW-DF2 curve (green) displays higher adsorption energies which are more realistic as the number of layers of P (and thus the larger the account of vanderWaals forces) increases.

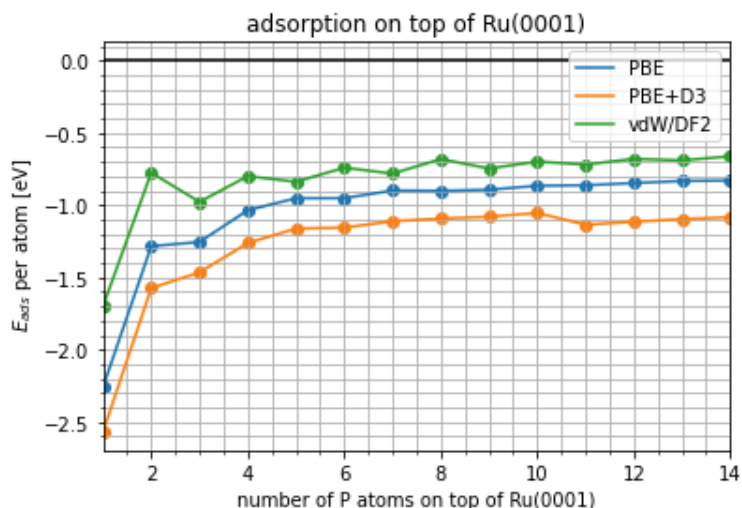


Figure 4.17: Adsorption energies per atom on a Ru(0001) surface. The x-axis represents the amount of P-layers on the surface.

#### 4.6.4. Structure

When moving from a two adsorption layer system to a system of more layers, the preferential stacking is lost and atoms will stick above each other in the current system. By placing monolayers of P on the  $1 \times 1$  surface unit cell of Ru(0001) in lateral directions DFT yields the energetics for monolayer growth. With each monolayer of P that is introduced on top of the previous one the adsorption per atom will decrease as shown in Figure 4.17. This process reaches a plateau value of about -1 eV after four to five layers as seen in Figure 4.17. Each next monolayer will bind similarly to the previous with all layers adsorbing. When the z-directions of these layers are observed more closely a trend is visible. The bond distance or z-height between the phosphorus monolayers are directly related to the number of layers and the position of the layer. An alternating pattern of a short distance (in the order of 2.2 Å) and a longer distance (in the order of 3.3 Å) is shown. This pattern is also directly related to the amount of layers present. In the situation where the third layer is introduced, the distance between the top two layers is large ( $>3.5$  Å). A bilayer is seen adhering to the surface with the top layer at a relatively large ( $>3$  Å) distance from this layer. When four phosphorus layers are on the surface there is a short bond between the top two and the bottom two layers, with a larger distance between these so called bilayers. In Figure 4.18 one can see that the bond between top two atoms ( $d_{01}$ ) is always short (2.2 Å) compared to the next bond between the second and third atom from the top ( $d_{12}$ ). This effect continues between the intra-bilayer bonds ( $d_{01}, d_{23}, d_{45}, d_{67}, d_{89}$ ) and inter-bilayer bonds ( $d_{12}, d_{34}, d_{56}, d_{78}, d_{910}$ ).

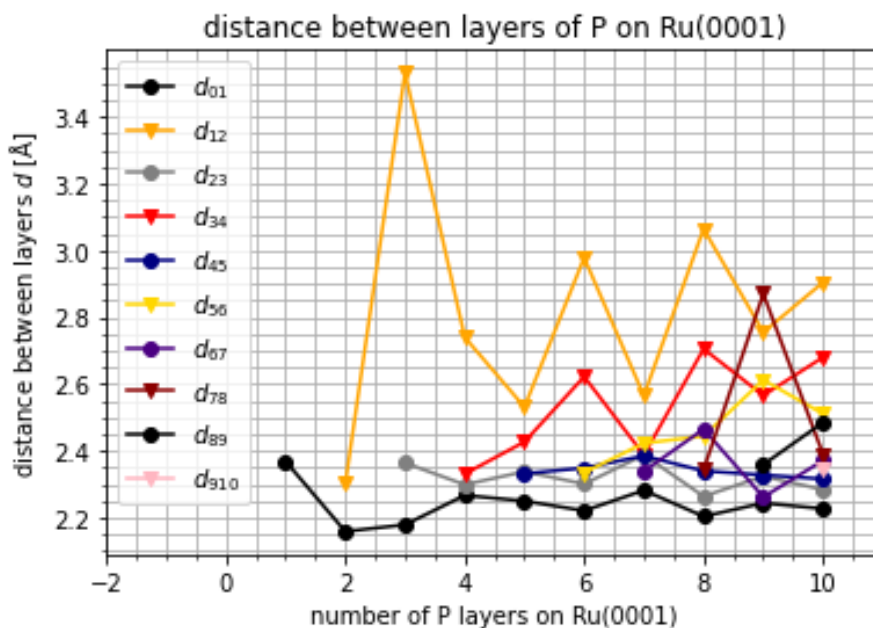


Figure 4.18: Distance between layers of P on Ru(0001). With  $d_{01}$  being the distance between the top 2 atoms, and  $d_{12}$  the distance between the second and third atom from the top. The distances labeled with dots represent an intra-bilayer distance. The distances labeled with triangles represent an inter-bilayer distance. Values are made with the XC-functional being PBE.

To formulate the trend of bilayer formation the distances between the adsorbed layers are analysed for the systems with one monolayer of P till ten monolayers of P on the Ru(0001) surface. This is done for three described XC approaches (PBE, PBE+D3 and vdW-DF2). In Figure 4.18 the distances between monolayer pairs are plotted for the systems with one monolayer till ten monolayers adsorbed. What is clear is that the distance between the top two atoms is the shortest in any simulated situation. This can be explained by the dangling bonds that the top atoms at the top side will have, leading to stronger binding to the layer below it, leading to the short bonds. The next two atom pairs show a longer bond in any of the situations. When the next atom pair is observed we again see a short bond distance. Below that again a longer bond distance. This pattern is repeated throughout the adsorbed layers and present in using all XC approaches. The differences do weaken as more and more layers are introduced, approaching a more bulk-like behaviour. There is however a strong bilayering trend visible in the ten layer adsorbed system.

## 4.7. Phosphorus bilayers

The hypothesis that bilayers of P form on top is analyzed further by disentangling bonding contributions within (intra) and between (inter) two bilayers. Figure 4.19 shows this schematically. The different bonds shown are also denoted by the small letter  $d$  (for intra-bilayer) and capital letter  $D$  (for inter-bilayer).

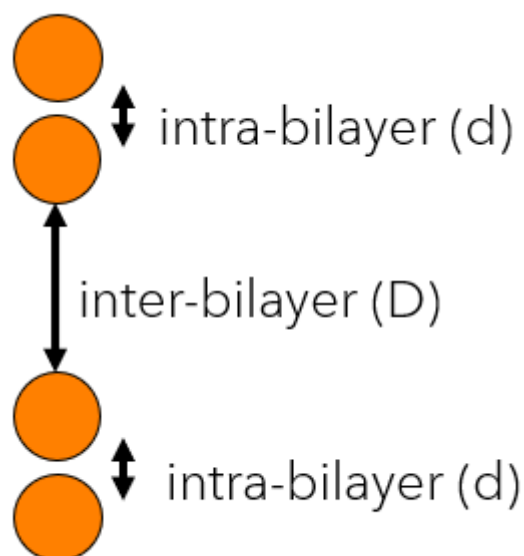


Figure 4.19: Distinction between inter- and intra-bilayers and their bond lengths  $D$  and  $d$  respectively.

#### 4.7.1. Intra and interlayer bonding

To investigate whether the phosphorus atoms do show an onset of growth through bilayering in the system, we have to verify the interactions of bonds within and between bilayers of phosphorus. This is done in a separate study without the ruthenium slab. Four P atoms are considered in every calculation with varying distances between and within bilayers. In the first simulation the distance between the bilayers is fixed, while the outer two atoms were free to move. This way a set of simulations can be done to check how the intra-bilayer distance ( $d$ ) is dependant on the inter bilayer distance ( $D$ ). Also the 1D potential energy curve of the inter-bilayer distance can be found using this method. It is repeated using PBE, PBE+D3 and vdW-DF2. The black zero line in Figure 4.20 displays the energy of two separated bilayers at a large distance from each other.

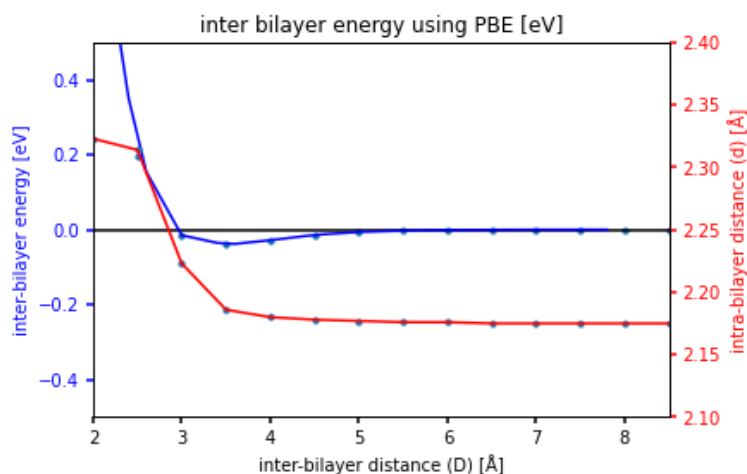


Figure 4.20: Binding energy and intra-bilayer distances for different inter-bilayer bond lengths using the PBE functional.

What can be seen looking at Figure 4.20 is that there is a trade off in optimal distances  $D$  and  $d$ . The point at which the lowest energy is found (at 3.5 Å between bilayers reaching -40 meV) the optimal bond length of the bilayer (d) is not yet reached (with a value of 2.18 Å at the right axis). The optimal bond is shown schematically in Figure 4.21 with B. At high values of  $x$ , the bilayers are completely separated and can be assumed to have no interaction with each other. This is shown in Figure 4.21 with Figure C. At the left end of the graph where values of  $D$  are small the middle two atoms are treated

as a bilayer and the distance of the outer two atoms will be large. This is shown in Figure 4.21 with the letter A. As the system moves between the two one can see a potential well, where the energy is lowest due to the interaction between the bilayers.

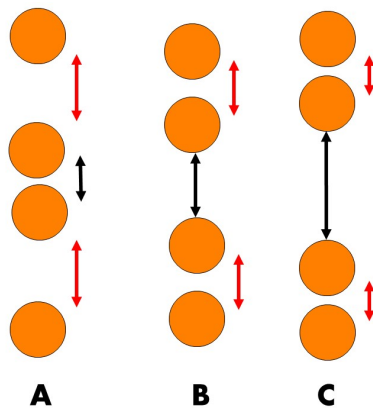


Figure 4.21: Schematic description of situation of bilayering in phosphorus layers. Distance  $D$  shown in black and distance  $d$  shown in red. Situation A shows a single bilayer, B the optimal positions of two bilayers, and C the long distance position of two bilayers.

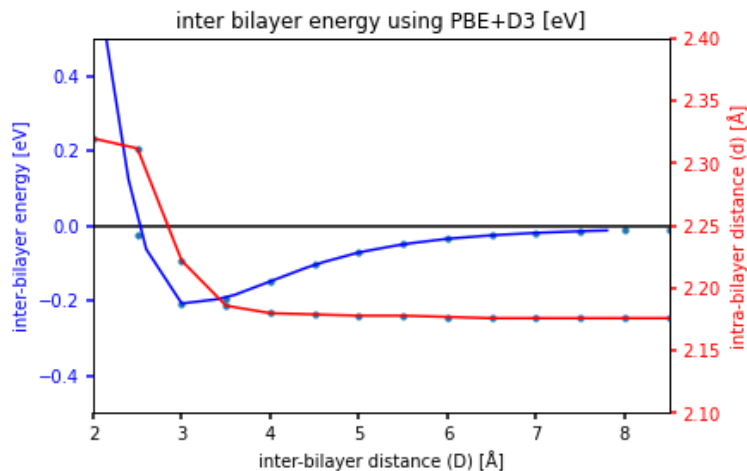


Figure 4.22: Binding energy and intra-bilayer distances for different inter-bilayer bond lengths using the PBE functional with the D3 correction.

When looking at the same simulation using PBE with the dispersion correction in Figure 4.22, we can see a the same picture again. The energetic optimum however is lower at -200 meV and the optimum inter bilayer distance is shorter at around 3 Å. This is as to be expected because of the additional vdW contributions to the bonding that are accounted for on top of PBE. The intra-bilayer distance however is similar to PBE at 2.18 Å.

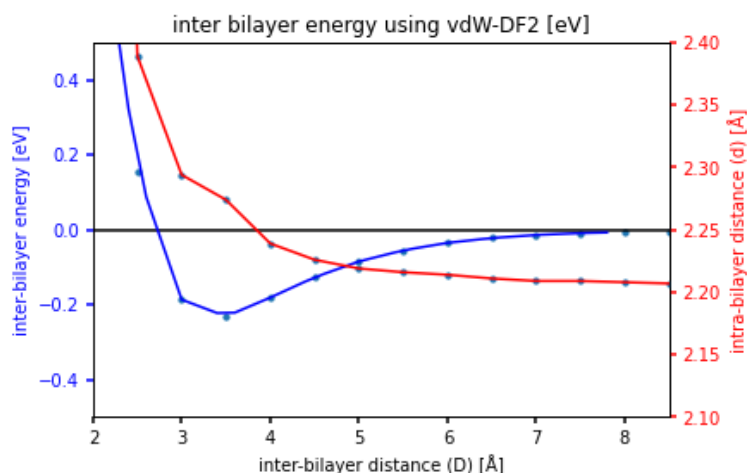


Figure 4.23: Binding energy and intra-bilayer distances for different inter-bilayer bond lengths using the vdW-DF2 functional.

As shown in Figure 4.23 vdW-DF2 follows the trend. The optimum interlayer distance  $D$  corresponds more to the result obtained with PBE. The depth of the potential well is in agreement with the results using PBE+D3. The depth of the well using the vdW-DF2 functional is -210 meV. The bond length of the intra-bilayer bond is 2.21 Å and thus slightly larger compared to PBE and PBE+D3. What can also be seen in Figure 4.23 is that there is a large repulsion part shown for the bond  $d$  when  $D$  is small. In the left part of the Figure  $D$  is approaching a small value where the middle two atoms can be interpreted as a bilayer, the outer two atoms then move away. Using vdW-DF2 this distance  $d$  is actually increasing to a value higher than 2.4 Å. For the other two methods (PBE and PBE+D3) this bond length  $d$  plateaus.

To study the effect these layers have on each other one can look at the separate bond types. To achieve this two separate sets of simulations are conducted. The ideal intra-bilayer distance can be determined by a simulation with only two P atoms in the unit cell. Varying their distance then yields a one-dimensional potential energy curve. From the minimum of this curve the ideal bond distance and interaction energy can be read. The simulation for intra-bilayer binding energy is done using two atoms instead of the previous four atom systems. In Figure 4.24 the simulation of the intra-bilayers bond  $d$  is denoted by the red border.

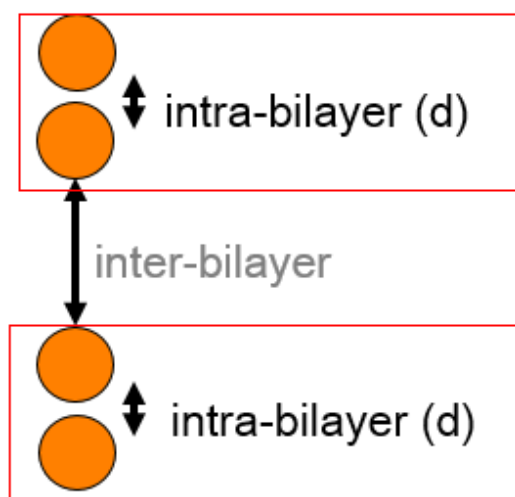


Figure 4.24: Bilayer schematic showing intra-bilayer bond  $d$ .

The binding energy between two bilayers of phosphorus in the Ru(0001) lattice is shown in Figure 4.25. The curves are plotted for the systems using PBE, PBE+D3 and vdW-DF2. The dots represent the data and the curve is obtained by linear fitting. The black dots represent the relaxed optimal position

and thus the minimum of the potential curve. The optimal bond length of bilayers is the same for PBE and PBE+D3 at 2.18 Å, the vdW-DF2 functional has a slightly higher estimated bond length of 2.28 Å. Intra-bilayer binding energies of -1.04, -1.47 and -1.57 eV are found using PBE, PBE+D3 and vdW-DF2 respectively. Here the difference between taking VanderWaals bonding into account or not are approximately 500 meV. Both PBE and PBE+D3 result in about the same bond length, which is slightly shorter than that using vdW-DF2 indicating that they are likely overbinding.

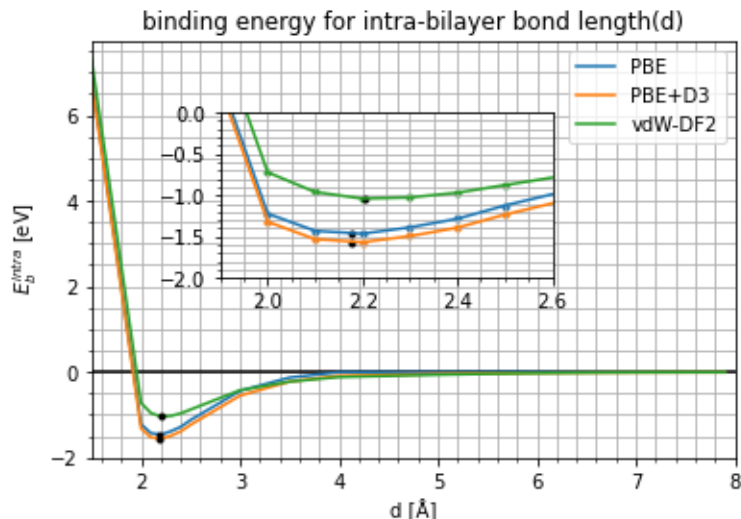


Figure 4.25: Binding energy curves of P-bilayers using PBE, PBE+D3 and vdW-DF2.

Having found the optimal bond length and binding energy for bilayers also the interlayer binding can be analyze further. This has to be done using four P atoms above each other to simulate a single inter-bilayer bond D. The calculation is set up by fixing the middle two atoms in set intervals. The outer two atoms were relaxed in the z-direction. In Figure 4.26 one can see the boundaries of the fixed system denoted by the red border, and the relaxed system, denoted by the blue border. In the case of the black dots in Figure 4.27 all four atoms are relaxed in z-direction.

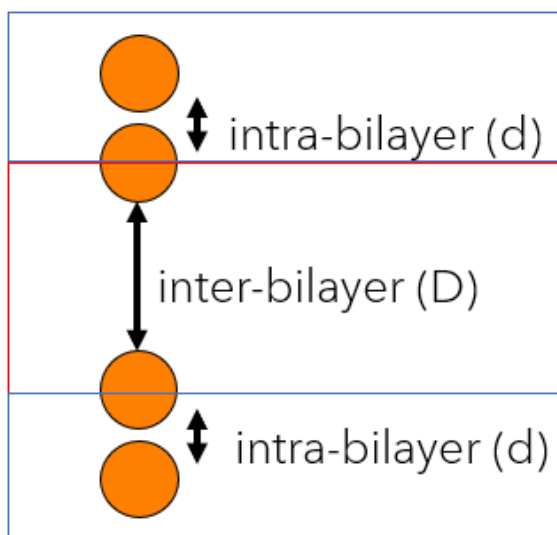


Figure 4.26: schematic showing boundary of simulation of inter-bilayers D.

The plotted one dimensional potential curves in Figure 4.27 display the bond distance of inter-bilayers D and energetic contribution. These values are taken by subtracting two times the intra-bilayer

energies from the system. If the minimum of the potential curve would show the same optimal bond length as seen in Figure 4.25, then this would be an indication that the stacking does not follow a pattern of bilayers but somewhat of an homogeneous stacking instead. This is however not the case. The optimal distance between two relaxed bilayer bonds is a larger bond with a shallow energy well. The binding between bilayers is optimal at distance  $D = 3.38, 3.11$  and  $3.37$  Å for PBE, PBE+D3 and vdW-DF2 respectively. So the system of four monolayers above each other in a Ru(0001) lattice will form two sets of bilayers above each other. The binding energy between these bilayers is significantly smaller compared to the intra-bilayer bonding. The optimal binding energy between bilayers is  $-4, -210$  and  $-240$  meV for PBE, PBE+D3 and vdW-DF2 respectively. Here the distinction between the methods that take vanderWaals forces into account (vdW-DF2, and through correction PBE+D3) and the one that does not (PBE) is significant. Where the value of the interaction using PBE is almost negligible, the other two methods do account for an interaction. The difference is in the range of 200 meV and therefore not to be neglected.

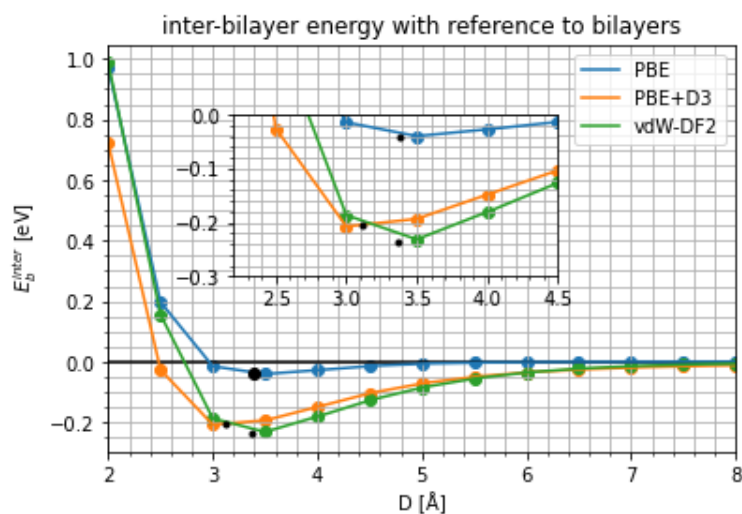


Figure 4.27: Binding energy curves between 2 P bilayers using three methods.

### 4.7.2. SB2M-formula

As shown in the previous sections, due the formation of bilayers with intra- and interbilayer bonding contributions, there is no passivation of the Ru(0001) by (continued) adsorption of phosphorus. This raises the question:

Can we describe the adsorption of monolayers of P on a Ru(0001) surface analytically through bilayer interactions?

The two different bilayer interactions together with surface and interface interactions are used to develop a simple analytical formula named SB2M. The name is derived from Surface, 2 types of bilayer interactions and the letter M for method.

Since all work has been conducted in  $1 \times 1$  surface unit cells, there are no conclusions to be drawn for larger systems. The value of inter-bilayer binding energy using PBE is 4 meV, which is at the limit of the accuracy of the underlying DFT calculations. Therefore, the effective interaction parameters obtained in the following can be expected to be most meaningful for the two functionals that include vdW interactions (PBE+D3 and vdW-DF2). The dispersion correction also has a cutoff after a set distance of 20 Å and will therefore not take into account atoms further away.

surface interaction

It is assumed that the energetic contribution of the surface is always the same independent of the simulation as long as we are dealing with the same surface. This surface contribution can therefore be taken as a fixed value  $E_{surf}$ . This contribution comes from the simulation with 0 adsorbate atoms.

### interface interaction

As the first monolayer is likely to bind stronger to the surface than every next layer, we assume there to be a fixed value of binding between the Ru(0001) surface and the first monolayer. The first monolayer of P binds on the surface with a binding energy  $E_{interface}$  of -1.52, -1.78 and -1.18 eV for PBE, PBE+D3 and vdW-DF2 respectively.

### Intra-bilayer interaction

The intra-bilayer bonding found in section 4.7 are in the order of magnitude of an eV. For every two atoms of P on top of the Ru(0001) surface one can assume there to be one unit of  $E_{bilayer}$  present. To be continuous the bilayer binding energies are added in steps of 0.5 to take monolayers into account. The binding energies for bilayers are -1.47, -1.57 and -1.04 eV for PBE, PBE+D3 and vdW-DF2 respectively.

### Inter-bilayer interaction

$E_{inter-bilayer}$  is taken as the optimal binding energy of the inter-bilayer bond found in the section 4.7. For PBE, PBE+D3 and vdW-DF2 the values are -4, -210 and -240 meV respectively. Multiple approaches can be made for accounting the amount of inter-bilayers present in a system with a given number of layers P. An approach would be that for every layer there has to be half an inter-bilayers present. One can however also note that the first inter-bilayer would have to be present when the third layer of P is added as seen in P-O-P systems (4.6.2). This would also account for a full inter-layer present when the top atom is not a bilayer yet, as is the case in three atoms. And after that the inter-bilayer would appear every other layer. These two different approaches for counting inter-bilayer bonds are denoted by A and B. In Figure 4.28 the amount of inter-bilayers that are accounted for are shown. At even layers of P on the Ru(0001) surface the values using A and B are the same.

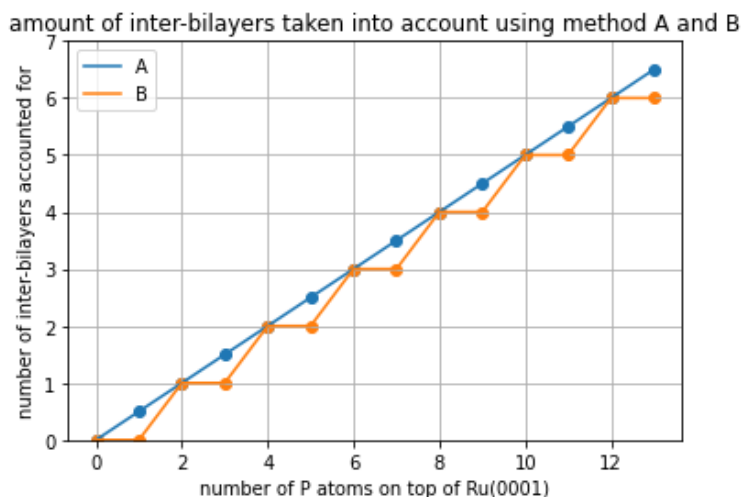


Figure 4.28: Amount of inter-bilayers taken into account using methods A and B.

When the sum of binding (both to the surface and to each other) is added up, what is left is the equation of the method that estimated the energetic outcome of the VASP simulations. This can be written in the form of:

$$E_{total} = E_{surf} + E_{interface} + 0.5 * N * E_{bilayer} + x * N * E_{inter-bilayer}. \quad (4.1)$$

In this equation  $N$  represents the number of P layers adhering to the Ru(0001) surface. Scaling factor  $x$  represents the method A or B in calculating the amount of inter-bilayers, with  $x=0.5$  for A and  $x=+1$  for every two layers starting at 3. When the results from the analytical method are compared to the outcome of the simulations of monolayers P on top of the Ru(0001) surface, a clear trend is visible. In Figure 4.29 the absolute difference is shown between the simulation and analytical method. Method A is shown as SB2M and method B is named SB2M+. The Figure shows that at larger number of layers ( $> 8$  layers) the SB2M and SB2M+ methods are very good at describing the outcome of simulations. At fourteen atoms (the largest tested system) all values are within 50 meV of the simulation outcome. At

the lower end of the graph there are some differences present between the SB2M(+) method and the simulations. At two atoms the formula assumes there to be one bilayer present and the interface and surface contributions. The first adsorbed layer of phosphorus however is strongly binding to the surface so its contribution to the bilayer is likely to be smaller. This explains the overshoot in the analytical formula seen at 2 layers adsorbed on the surface in Figure 4.29. In Figure 4.30 the adsorption is shown for the simulations (dots) and the analytical formula (lines). It is visible that the formula is excellent at predicting the adsorption from the simulation. The PBE+D3 outcome is described within 10 meV of the simulation for systems with more than 12 layers of P on the surface as can be seen in Figure 4.29.

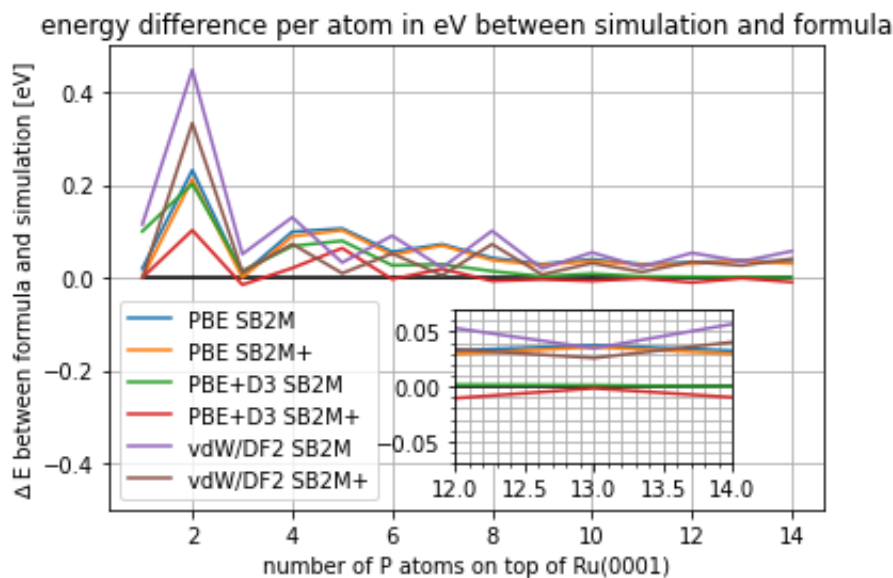


Figure 4.29: Difference between simulations and SB2M(+) method for systems of P overlayers on the surface.

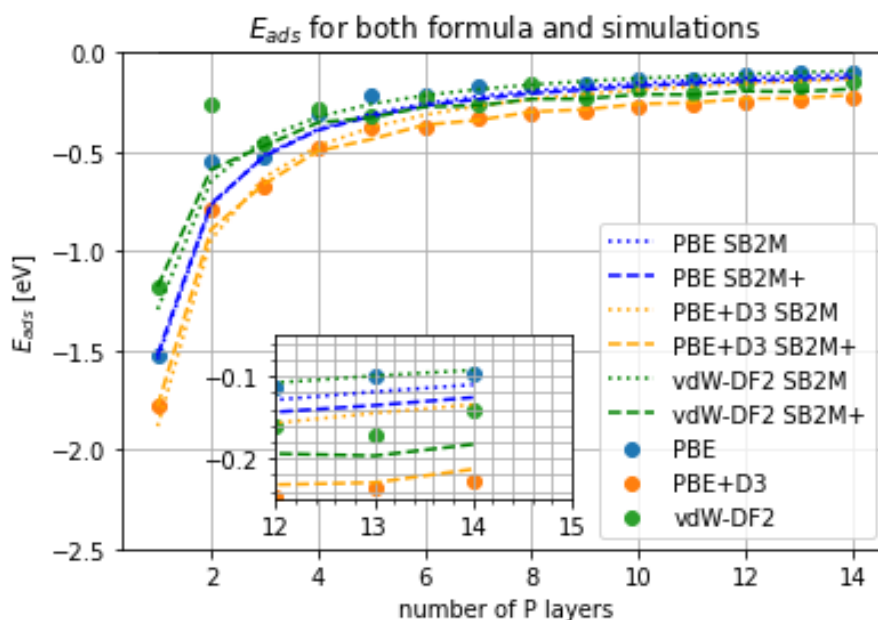


Figure 4.30: Adsorption energies of VASP simulation (dots) and SB2M(+) formula (lines).



# 5

## Conclusions, Summary and Outlook

### 5.1. Conclusions

In conclusion the single-layer co-adsorption of phosphorus and oxygen and multilayer adsorption of phosphorus on Ru(0001) has been studied based on 1x1 surface unit cells in this work. The latter has been found to be well described by P-P bilayer formation, which allows to describe the adsorption energetics by a simple analytical formula (coined SB2M). To come back to the main research question:

**How does phosphorous overlayers adsorb on a Ru(0001) surface, and what is the mechanism of multi-layer growth?**

We can say that a monolayer of phosphorus is bound via the hcp site with an adsorption energy of around 1 eV compared to a free-standing phosphorus film with the same lateral periodicity. The growth in full monolayer coverage regime will be dominated by bilayering with plateauing binding energies upon continued growth. In all situations the preferred site for adhesion is the hcp-hollow site for P to adhere to the Ru(0001). Comparing the adsorption energies, the site preference is hcp, fcc, bridge and top. Initial adsorption of the overlayer and second monolayer of P atoms on the Ru(0001) follow the pattern hcp-fcc, with differences in second site preference are below 500 meV. When more than two layers of atoms are adsorbed to the surface, stacking preferences are lost in all but the first adsorbing layer. Every layer above it are stacked on top of the first one. The binding energy of the second monolayer of P atoms on the surface is 1 eV per atom higher than that of the initial adsorption. This value goes up till it plateaus around the fourth layer binding with about 1 eV per atom. The continued adsorption of phosphorus tends to form bilayers stacked on top of each other bound by (relatively weak) vanderWaals forces. The intra-bilayer bonds have a binding energy in the range of 1.5 eV where the inter-bilayer bonds have a weaker 200 meV binding energy mainly dominated by vanderWaals forces. When going to coverages with  $\theta < 1$  ML, the adsorption per atom is higher due to reduced lateral repulsion by other P atoms. The coverage dependence of P on Ru(0001) is similar to that of O on Ru(0001) The simulation of P layers added to a Ru(0001) surface can be described well using a simple analytical summation of bilayer and inter-bilayer interactions. This has been described in the SB2M and SB2M+ formulae.

### 5.2. Summary

The adsorption mechanism of phosphorus on a ruthenium (0001) surface has been studied based on first-principles simulations using 1x1 surface unit cells. The bulk structures and atomisation energies of phosphorus oxides are simulated. Possible supercells needed for adsorption of two dimensional phosphorene (oxide) structures on a Ru(0001) surface with minimised strain are investigated. Density functional theory (DFT) calculations were performed to find optimal adsorption sites on a Ru(0001) surface for both P and O. The result was a clear picture of four high coordination sites and a preference for oxygen to adsorb on the surface compared to phosphorus on a same site basis. The four high coordination positions were then used to test possible stacking positions for multiple layers. Upon stacking more phosphorus layers, the adsorbate layer follows a pattern of 'on top' stacking with alternating layer heights. The layer distances and adsorption energetics show a tendency to form bilayers. A separate study investigating binding energies of these bilayers is done to confirm the hypothesis showing a

strong binding energy within bilayers of about 1.5 eV, and a weaker binding energy between bilayers of about 200 meV. A minimal analytical sum of binding interactions can be applied to the surface and bilayer energies showing an accurate description of the system.

### 5.3. Outlook

The results visible in chapter 4 show that the adsorption and onset of growth of P on Ru(0001) can be estimated very well using a summation of bilayer and inter-bilayer energies. However, this is based on considering 1x1 surface unit cells only for studying the adsorption, resulting in full monolayer coverage. So with any conclusion drawn one has to consider if this partly due to these lateral constraints. To get a better idea of this one can study the monolayer behaviour and growth using larger unit cells. Especially the potential lateral corrugation of the adsorbed layers can then be studied allowing to account for corrugated shapes as seen in phosphorene literature 3.3 or moiré patterns as seen in graphene overlayers 3.5.5. Scaling up the system will however cost considerable computing time that has to be accounted for. To investigate the use of Ru(0001) surfaces in both semiconductor industry as well as catalysts, one can expand the systems of Ru(0001) and P to include other or even more adsorbates. Additional research to the adhesion of P on other metal surfaces would greatly contribute to the fundamental knowledge of how atomic P behaves, as limited information about this is available.

One can study how well this bilayering scheme holds for adsorption on other metal surfaces. The Ru hcp structure is found in a range of other metals such as cobalt or zinc. From section ?? one can study the interfacial charge transfer of the other metal-P combinations.

A Ru surface can also be studied adsorbing other elements. In section 3.5 some other adsorbates are studied. These all show similar behaviour as described in section 4.5. When studying monolayers it can be concluded that the hcp-hollow site is preferred for adsorption. The surface is dominating the overlayer stacking sequence for all these combinations. The growth however has not been studied in detail for those systems.

The SB2M-formula is suited at describing the behaviour of monolayers of P on a ruthenium surface. It is however based on the results of section 4.7. This means that a small unit cells are small as discussed above. It is however not measured and parameterised to experimental data so it will likely not be able to draw conclusions in any real-life experimental situations.

As seen in the literature stable forms of phosphorus that could form are phosphorene and phosphorene oxides. Phosphorene has a corrugated structure that is not able to form in the small simulations performed in this work. The bond lengths however are close to those found in the system of stacked layers of P on a Ru(0001) surface. One could further investigate if these layers would form by using the results from the stacking of P atoms and initial study to supercell sizes for phosphorene adsorption. By performing simulations using a suitably large computational surface unit cell one could verify if phosphorene is likely to be the structure that forms when adding phosphorus to a Ru(0001) surface. The phosphorus bilayer simulations could also be repeated using larger cells to verify if indeed phosphorene, and upon more layers, black phosphorus would form.

The incorporation of oxygen in the stacking of phosphorus layers would give a better idea how the two atoms behave in relation to each other. In this work oxygen and phosphorus were both added to a Ru(0001) surface. The SB2M(+) method is however only applied for phosphorus on the metal surface. The extension to oxygen can be made by increasing the cell size and repeating calculations doped with oxygen atoms. The modelling of oxygen does however impose additional challenges that have to be taken into account.

#### Relation to experimental data

Finally, it would be interesting to see whether some of the results of this study could be verified by experimental data obtained from appropriate surface science experiments. The initial step would be to investigate bonds of a Ru(0001) surface with an adhered layer of phosphorus on top experimentally about which more can be found in the appendix. The types of bonds and bond length can then directly be verified and related to the outcome of the simulation. The simulation on it's part can be parameterised semi-empirically to be closer related to the experimental outcome. If one has an isolated system experimentally and can use the values as input in the simulation, then the simulation will be more precise in predicting experimental outcome for systems closely related.

# 6

## Appendix

### 6.1. Experimental techniques

Though experimental methods are not used in this study, there is relevance if one wants to link the computational work to experiments. Therefore most relevant experimental characterisation methods for measuring adsorption are briefly mentioned below.

In order to study adsorption of P on Ru(0001) one can use various methods of characterisation. Not only computational methods are needed to study at the atomic scale. While experimental measurements are increasingly difficult to perform with decreasing scale size (unlike computational methods) there are options available. Since the full report will cover computational work only, not too much emphasis is given to experimental outcomes. Some experimental techniques used in surface science are however suited to relate to computational results. Most notably found in comparison to DFT results is Low-Electron Energy Diffraction (LEED). In this technique the electrons with energies of 20-200 meV are used to be scattered inelastically by the first few layers of the surface. Not only qualitative characterisation can be done this way (through the diffraction pattern revealing the symmetry of the unit cell), but also quantitative through the positions of the atoms in the crystal [94]. This makes the characterisation technique especially suited to determine bond lengths and strain within a surface. Another method suited for surface characterisation is Auger Electron Spectroscopy (AES). In this method the removal of K-shell electrons from the surface causes the surface to relax by having an electron from a higher state to fall back to the core shell and emitting an Auger electron in the process. Since the technique is highly sensitive it is especially suited for surface science. It can give an accurate quantitative description of the composition of the first layers of the surface [18]. If one wants to look at exact cross-sections of surfaces at the atomic scale one could use Scanning Tunneling Microscopy (STM). There a metallic probe is hovered above the surface with an applied voltage. Tunneling of the electrons between the surface and probe causes a measurable current. This current can map the electronic structure of the surface of the sample. The ability to accurately display lengths at atomic scale makes STM suited for verifying growth of adsorbates [67].

Other experimental methods are of course present in many works on adsorption, these are however most relevant to compare to DFT results of adsorption on a Ru(0001) surface.

### 6.2. A 2D materials fit

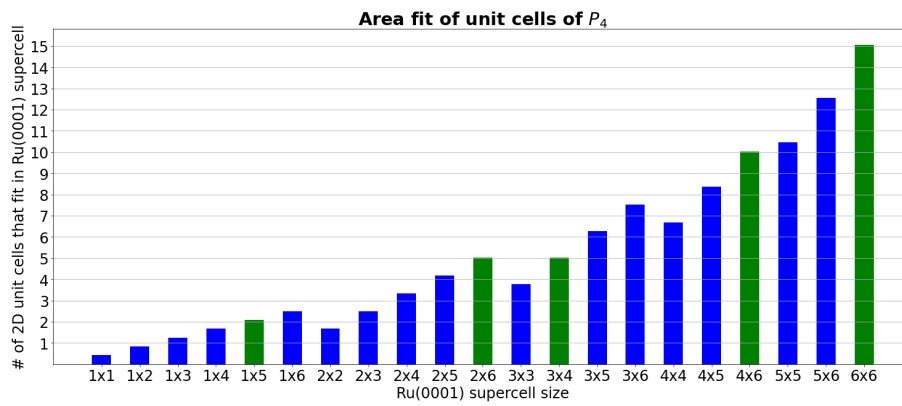
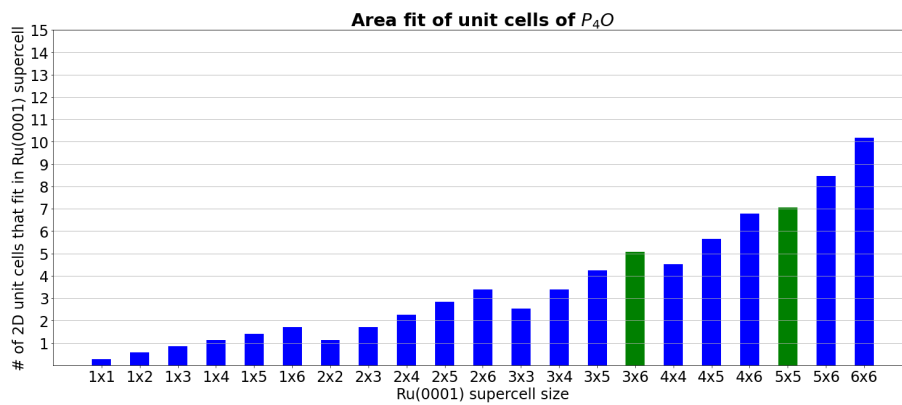
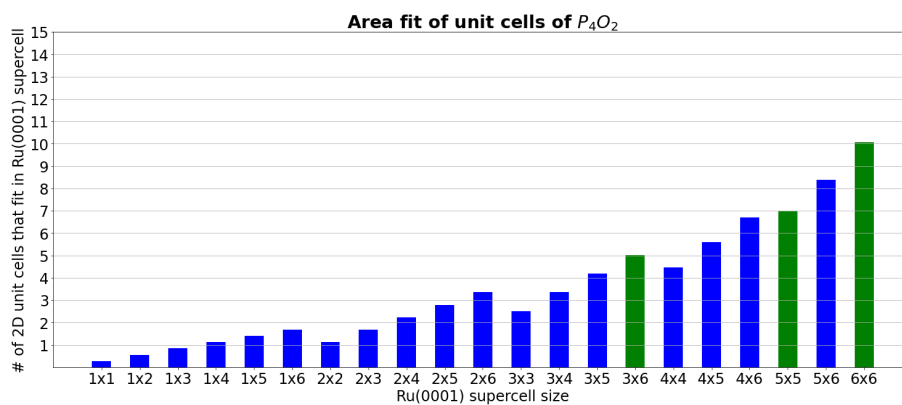


Figure 6.1: Phosphorene

Figure 6.2: phosphorene oxide  $P_4O$ Figure 6.3: phosphorene oxide  $P_4O_2$

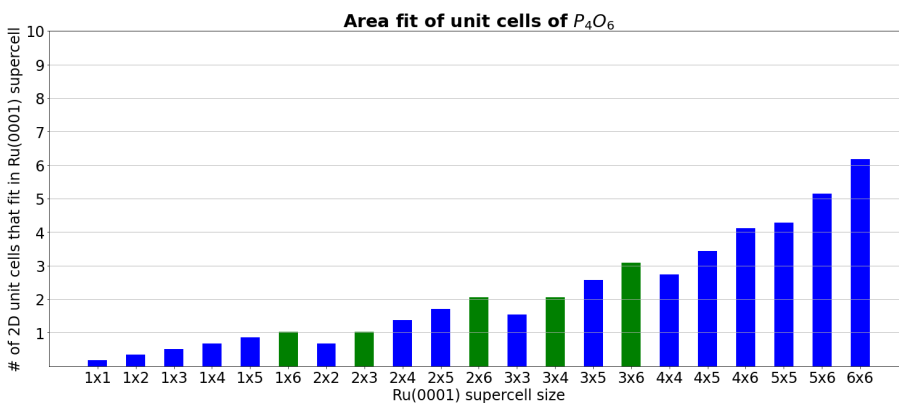


Figure 6.4: phosphorene oxide P4O6

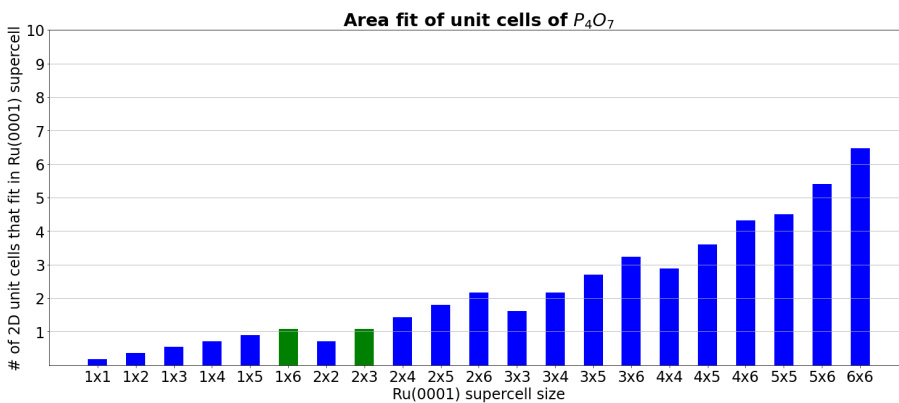


Figure 6.5: phosphorene oxide P4O7

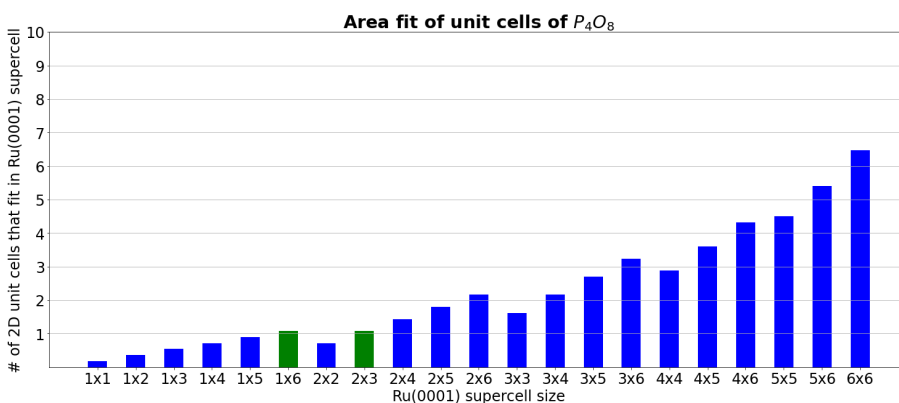


Figure 6.6: phosphorene oxide P4O8

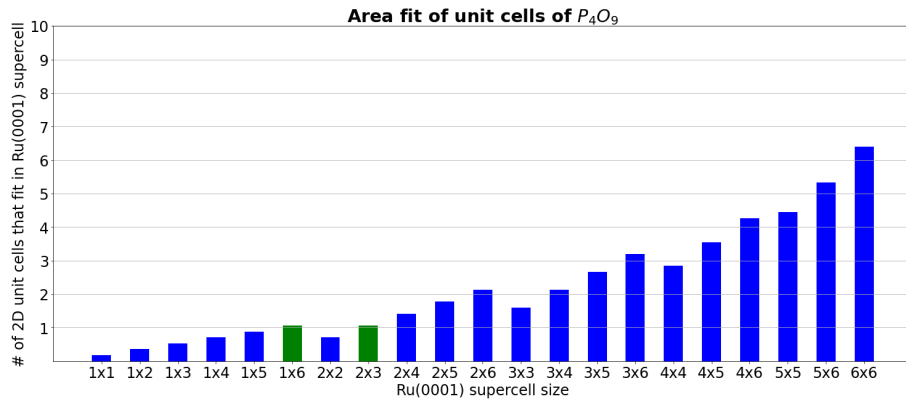


Figure 6.7: phosphorene oxide P4O9

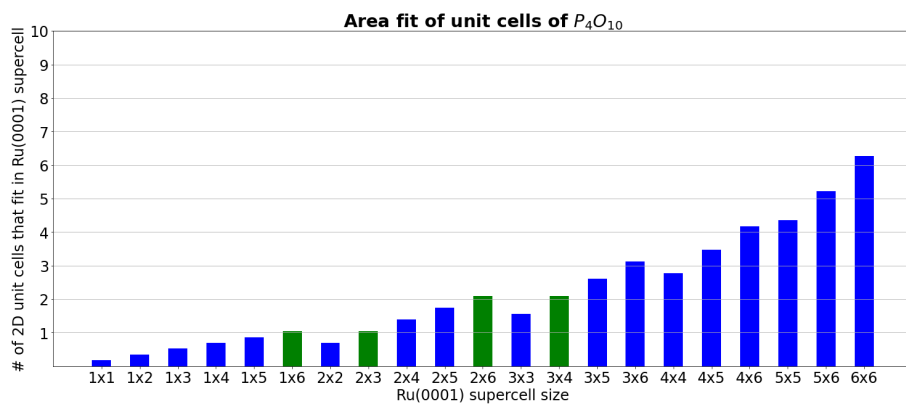


Figure 6.8: phosphorene oxide P4O10

# Bibliography

- [1] Yohannes Abate, Deji Akinwande, Sampath Gamage, Han Wang, Michael Snure, Nirakar Poudel, and Stephen B Cronin. Recent Progress on Stability and Passivation of Black Phosphorus. *Advanced Materials*, 30(111):1704749, 2018. doi: 10.1002/adma.201704749.
- [2] Richard I. Ainsworth, Devis Di Tommaso, and Nora H. De Leeuw. A density functional theory study of structural, mechanical and electronic properties of crystalline phosphorus pentoxide. *Journal of Chemical Physics*, 135(23), 2011. doi: 10.1063/1.3666017.
- [3] El Hassan Arbib, Brahim Elouadi, Jean Pierre Chaminade, and Jacques Darriet. New refinement of the crystal structure of  $\alpha$ -P<sub>2</sub>O<sub>5</sub>. *Journal of Solid State Chemistry*, 127(2):350–353, 1996. doi: 10.1006/jssc.1996.0393.
- [4] John W. Arblaster. Crystallographic properties of ruthenium. *Platinum Metals Review*, 57(2): 127–136, 2013. doi: 10.1595/147106713X665030.
- [5] Richard F. W. Bader. *Atoms in Molecules*. Clarendon Press, 1994. ISBN 9780198558651.
- [6] Jakub D. Baran, Henrik Grönbeck, and Anders Hellman. Mechanism for limiting thickness of thin oxide films on aluminum. *Physical Review Letters*, 112(14):1–5, 2014. doi: 10.1103/PhysRevLett.112.146103.
- [7] Raoul Blume, Horst Niehus, Horst Conrad, Artur Böttcher, Lucia Aballe, Luca Gregoratti, Alexei Barinov, and Maya Kiskinova. Identification of subsurface oxygen species created during oxidation of Ru(0001). *Journal of Physical Chemistry B*, 109(29):14052–14058, 2005. doi: 10.1021/jp044175x.
- [8] Cindy Bogaart. *Potential Energy Surfaces for Coverage Dependent Diffusion of O on Ru (0001): A Density Functional Theory Study [Bsc. Thesis]*. Universiteit Leiden, 2020.
- [9] Artur Böttcher and Horst Niehus. Formation of subsurface oxygen at Ru(0001). *Journal of Chemical Physics*, 110(2-12):3186–3195, 1999. doi: 10.1063/1.477839.
- [10] Artur Böttcher and Horst Niehus. Oxygen adsorbed on oxidized Ru(0001). *Physical Review B*, 60(20):14396–14404, 11 1999. doi: 10.1103/PhysRevB.60.14396.
- [11] David R Bowler and Angelos Michaelides. Van der Waals density functionals applied to solids. pages 1–29, 2011.
- [12] Thomas Brugger, Sebastian Günther, Bin Wang, J. Hugo Dil, Marie-Laure Bocquet, Jürg Osterwalder, Joost Winterlin, and Thomas Greber. Comparison of electronic structure and template function of single-layer graphene and a hexagonal boron nitride nanomesh on Ru(0001). *Physical Review B*, 79(4):045407, 1 2009. doi: 10.1103/PhysRevB.79.045407.
- [13] Sheneve Z. Butler, Shawna M. Hollen, Linyou Cao, Yi Cui, Jay A. Gupta, Humberto R. Gutiérrez, Tony F. Heinz, Seung Sae Hong, Jiaying Huang, Ariel F. Ismach, Ezekiel Johnston-Halperin, Masaru Kuno, Vladimir V. Plashnitsa, Richard D. Robinson, Rodney S. Ruoff, Sayeef Salahuddin, Jie Shan, Li Shi, Michael G. Spencer, Mauricio Terrones, Wolfgang Windl, and Joshua E. Goldberger. Progress, challenges, and opportunities in two-dimensional materials beyond graphene. *ACS Nano*, 7(4):2898–2926, 2013. doi: 10.1021/nn400280c.
- [14] N Cabrera and N F Mott. Theory of the oxidation of metals. *Reports on Progress in Physics*, 12 (163), 1949.

- [15] Alexandra Carvalho, Min Wang, Xi Zhu, Aleksandr S. Rodin, Haibin Su, and Antonio H. Castro Neto. Phosphorene: From theory to applications. *Nature Reviews Materials*, 1(11), 2016. doi: 10.1038/natrevmats.2016.61.
- [16] Andres Castellanos-Gomez, Leonardo Vicarelli, Elsa Prada, Joshua O. Island, K. L. Narasimha-Acharya, Sofya I. Blanter, Dirk J. Groenendijk, Michele Buscema, Gary A. Steele, J. V. Alvarez, Henny W. Zandbergen, J. J. Palacios, and Herre S.J. Van Der Zant. Isolation and characterization of few-layer black phosphorus. *2D Materials*, 1(2), 2014. doi: 10.1088/2053-1583/1/2/025001.
- [17] D. M. Ceperly and B J Alder. Ground State of the Electron Gas by a Stochastic Method. *Physical Review Letters*, 45(7):566–569, 1980.
- [18] Chuan C. Chang. Auger electron spectroscopy. *Surface Science*, 25(1):53–79, 3 1971. doi: 10.1016/0039-6028(71)90210-X.
- [19] Y. S. Chang and M. L. Chou. Formation and structure of epitaxial ruthenium silicides on (111)Si. *Journal of Applied Physics*, 68(5):2411–2414, 1990. doi: 10.1063/1.346500.
- [20] Hui Chen, Xuan Ai, Wang Liu, Zhoubing Xie, Weiqiang Feng, Wei Chen, and Xiaoxin Zou. Promoting Subordinate, Efficient Ruthenium Sites with Interstitial Silicon for Pt□Like Electrocatalytic Activity. *Angewandte Chemie*, page ange.201906394, 7 2019. doi: 10.1002/ange.201906394.
- [21] William Chou, Leo Chen, Jennifer Shao, Andrew Chen, Roger Chung, and Lisa Zhou. Semiconductors – the Next Wave, Opportunities and winning strategies for semiconductor companies. *Deloitte*, (April):1–58, 2019.
- [22] D. W. J. Cruickshank. Refinements of structures containing bonds between Si, P, S or Cl and O or N. VI. P 2 O 5 , form III. *Acta Crystallographica*, 17(6):679–680, 6 1964. doi: 10.1107/S0365110X64001682.
- [23] L. R. Danielson, M. J. Dresser, E. E. Donaldson, and J. T. Dickinson. Adsorption and desorption of ammonia, hydrogen, and nitrogen on ruthenium (0001). *Surface Science*, 71(3):599–614, 1978. doi: 10.1016/0039-6028(78)90450-8.
- [24] H. Dietrich, K. Jacobi, and G. Ertl. Coverage, lateral order, and vibrations of atomic nitrogen on Ru(0001). *The Journal of Chemical Physics*, 105(19):8944–8950, 11 1996. doi: 10.1063/1.472624.
- [25] M. Dion, H. Rydberg, E. Schröder, D. C. Langreth, and B. I. Lundqvist. Van der Waals density functional for general geometries. *Physical Review Letters*, 92(24):22–25, 2004. doi: 10.1103/PhysRevLett.92.246401.
- [26] John F. Dobson, Angela White, and Angel Rubio. Asymptotics of the dispersion interaction: Analytic benchmarks for van der Waals energy functionals. *Physical Review Letters*, 96(7):4–7, 2006. doi: 10.1103/PhysRevLett.96.073201.
- [27] Emre Emmez, Bing Yang, Shamil Shaikhutdinov, and Hans Joachim Freund. Permeation of a single-layer SiO<sub>2</sub> membrane and chemistry in confined space. *Journal of Physical Chemistry C*, 118(50):29034–29042, 2014. doi: 10.1021/jp503253a.
- [28] Emre Emmez, J. Anibal Boscoboinik, Samuel Tenney, Peter Sutter, Shamil Shaikhutdinov, and Hans Joachim Freund. Oxidation of the Ru(0001) surface covered by weakly bound, ultrathin silicate films. *Surface Science*, 646:19–25, 2016. doi: 10.1016/j.susc.2015.06.019.
- [29] Venkataramana Erapalapati, Umatai A Hale, and Nandita Madhavan. Phosphorus pentoxide for amide and peptide bond formation with minimal by-products. *Tetrahedron Letters*, 60(49):151311, 2019. doi: 10.1016/j.tetlet.2019.151311.

- [30] Xiangmin Fei, Joshua Neilson, Yanbang Li, Vanessa Lopez, Simon J. Garrett, Liangbing Gan, Hong Jun Gao, and Li Gao. Controlled Synthesis of Nitrogen-Doped Graphene on Ruthenium from Azafullerene. *Nano Letters*, 17(5):2887–2894, 2017. doi: 10.1021/acs.nanolett.7b00038.
- [31] Vivekanand V. Gobre and Alexandre Tkatchenko. Scaling laws for van der Waals interactions in nanostructured materials. *Nature Communications*, 4:1–6, 2013. doi: 10.1038/ncomms3341.
- [32] Jeff Greeley, Jens K. Nørskov, and Manos Mavrikakis. Electronic structure and catalysis on metal surfaces. *Annual Review of Physical Chemistry*, 53:319–348, 2002. doi: 10.1146/annurev.physchem.53.100301.131630.
- [33] Stefan Grimme, Jens Antony, Stephan Ehrlich, and Helge Krieg. A consistent and accurate ab initio parametrization of density functional dispersion correction (DFT-D) for the 94 elements H–Pu. *Journal of Chemical Physics*, 132(15), 2010. doi: 10.1063/1.3382344.
- [34] Stefan Grimme, Stephan Ehrlich, and Lars Goerigk. Effect of the damping function in dispersion corrected density functional theory. *Journal of Computational Chemistry*, 32(7):1456–1465, 5 2011. doi: 10.1002/jcc.21759.
- [35] M. Gsell, P. Jakob, and D. Menzel. Effect of substrate strain on adsorption. *Science*, 280(5364):717–720, 1998. doi: 10.1126/science.280.5364.717.
- [36] Junjie Guo, Jaekwang Lee, Cristian I Contescu, Nidia C Gallego, Sokrates T Pantelides, Stephen J Pennycook, Bruce A Moyer, and Matthew F Chisholm. Crown ethers in graphene. *Nature Communications*, 5(5389):1–6, 2014. doi: 10.1038/ncomms6389.
- [37] B. Hammer, L. B. Hansen, and J. K. Nørskov. Improved adsorption energetics within density-functional theory using revised Perdew–Burke–Ernzerhof functionals. *Physical Review B*, 59(11):7413–7421, 3 1999. doi: 10.1103/PhysRevB.59.7413.
- [38] G. C. Hampson and A. J. Stosick. The Molecular Structure of Arsenious Oxide, As<sub>4</sub>O<sub>6</sub>, Phosphorus Trioxide, P<sub>4</sub>O<sub>6</sub>, Phosphorus Pentoxide, P<sub>4</sub>O<sub>10</sub>, and Hexamethylenetetramine, (CH<sub>2</sub>)<sub>6</sub>N<sub>4</sub>, by Electro Diffraction. *Journal of the American Chemical Society*, 60(8):1814–1822, 1938. doi: 10.1021/ja01275a030.
- [39] Graeme Henkelman, Andri Arnaldsson, and Hannes Jónsson. A fast and robust algorithm for Bader decomposition of charge density. *Computational Materials Science*, 36(3):354–360, 2006. doi: 10.1016/j.commatsci.2005.04.010.
- [40] Jeffrey A. Herron, Scott Tonelli, and Manos Mavrikakis. Atomic and molecular adsorption on Ru(0001). *Surface Science*, 614:64–74, 2013. doi: 10.1016/j.susc.2013.04.002.
- [41] D. Heuer, T. Müller, H. Pfnür, and U. Köhler. Determination of the adsorption site of sulphur on Ru(0001) by STM. *Surface Science*, 297(1), 1993. doi: 10.1016/0039-6028(93)90006-6.
- [42] P. Hohenberg and W. Kohn. Inhomogeneous Electron Gas. *Physical Review*, 136(3B):B864–B871, 11 1964. doi: 10.1103/PhysRev.136.B864.
- [43] M. Jansen and M. Moebs. Structural investigations on solid tetraphosphorus hexaoxide. *Inorganic Chemistry*, 23(26):4486–4488, 12 1984. doi: 10.1021/ic00194a017.
- [44] Martin Jansen, Marlen Voss, and Hans-Jörg Deiseroth. Struktureigenschaften der Phosphoroxide im festen Aggregatzustand. *Angewandte Chemie*, 93(11):1023–1024, 11 1981. doi: 10.1002/ange.19810931127.
- [45] Q. X. Jia, S. G. Song, X. D. Wu, J. H. Cho, S. R. Foltyn, A. T. Findikoglu, and J. L. Smith. Epitaxial growth of highly conductive RuO<sub>2</sub> thin films on (100) Si. *Applied Physics Letters*, 68(8):1069–1071, 1996. doi: 10.1063/1.115715.
- [46] De En Jiang, Mao Hua Du, and Sheng Dai. First principles study of the graphene/Ru(0001) interface. *Journal of Chemical Physics*, 130(7):1–6, 2009. doi: 10.1063/1.3077295.

- [47] Il-Hwan Kim and Kwang-Bum Kim. Electrochemical Characterization of Hydrous Ruthenium Oxide Thin-Film Electrodes for Electrochemical Capacitor Applications. *Journal of The Electrochemical Society*, 153(2):A383, 2006. doi: 10.1149/1.2147406.
- [48] Jiri Klimeš, David R Bowler, and Angelos Michaelides. Chemical accuracy for the van der Waals. *Journal of Physics: Condensed Matter*, 22(2), 2009. doi: 10.1088/0953-8984/22/2/022201.
- [49] W. Kohn and L. J. Sham. Self-Consistent Equations Including Exchange and Correlation Effects. *Physical Review*, 140(4A):A1133–A1138, 11 1965. doi: 10.1103/PhysRev.140.A1133.
- [50] G. Kresse and J. Furthmüller. Efficiency of ab-initio total energy calculations for metals and semiconductors using a plane-wave basis set. *Computational Materials Science*, 6(1):15–50, 1996. doi: 10.1016/0927-0256(96)00008-0.
- [51] G. Kresse and J. Hafner. Ab initio molecular dynamics for open-shell transition metals. *Physical Review B*, 48(17):13115–13118, 1993. doi: 10.1103/PhysRevB.48.13115.
- [52] G. Kresse and J. Hafner. Norm-conserving and ultrasoft pseudopotentials for first-row and transition elements. *Journal of Physics: Condensed Matter*, 6(40):8245–8257, 1994. doi: 10.1088/0953-8984/6/40/015.
- [53] Vadym V. Kulish, Oleksandr I. Malyi, Clas Persson, and Ping Wu. Adsorption of metal adatoms on single-layer phosphorene. *Physical Chemistry Chemical Physics*, 17(2):992–1000, 2015. doi: 10.1039/C4CP03890H.
- [54] Xuefang. Lan. *Transition metal phosphides : synthesis and catalytic properties in hydrodesulfurization and hydrodeoxygenation*. 2018. ISBN 9789038644370.
- [55] Hyuck Lee, Mi Suk Cho, In Hoi Kim, Jae Do Nam, and Youngkwan Lee. RuOx/polypyrrole nanocomposite electrode for electrochemical capacitors. *Synthetic Metals*, 160(9-10):1055–1059, 2010. doi: 10.1016/j.synthmet.2010.02.026.
- [56] Jeong Gun Lee, Young Tae Kim, Suk Ki Min, and Sung Ho Choh. Effects of excess oxygen on the properties of reactively sputtered RuO<sub>x</sub> thin films. *Journal of Applied Physics*, 77(10):5473–5475, 1995. doi: 10.1063/1.359595.
- [57] Yutong Li, Fuqiang Chu, Yunfei Bu, Yong Kong, Yongxin Tao, Xiao Zhou, Haoran Yu, Junjie Yu, Lin Tang, and Yong Qin. Controllable fabrication of uniform ruthenium phosphide nanocrystals for the hydrogen evolution reaction. *Chemical Communications*, 55(54):7828–7831, 2019. doi: 10.1039/c9cc03668g.
- [58] Xi Ling, Han Wang, Shengxi Huang, Fengnian Xia, and Mildred S Dresselhaus. The renaissance of black phosphorus. *Proceedings of the National Academy of Sciences*, 112(15):4523–4530, 4 2015. doi: 10.1073/pnas.1416581112.
- [59] Da-chang Liu, Jin-ping Ni, Jun-xing Ye, Xiao-hui Ni, Xing-yuan Zhu, and Micro-arc Oxidation. and Evaluation Micro-arc Oxidation Coating Containing Phosphorus on Tantalum Substrates Prepared by. *Journal of Testing and Evaluation*, 2021. doi: <https://doi.org/10.1520/JTE20200647>.
- [60] Han Liu, Yuchen Du, Yexin Deng, and Peide D Ye. Semiconducting black phosphorus: synthesis, transport properties and electronic applications. *Chemical Society Reviews*, 2014. doi: 10.1039/C4CS00257A.
- [61] Jie Liu, Shunhong Zhang, Yaguang Guo, and Qian Wang. Phosphorus K 4 Crystal : A New Stable Allotrope. *Nature Publishing Group*, (October):1–9, 2016. doi: 10.1038/srep37528.
- [62] Tingting Liu, Bomin Feng, Xiuju Wu, Yanli Niu, Weihua Hu, and Chang Ming Li. Ru<sub>2</sub>P Nanoparticle Decorated P/N-Doped Carbon Nanofibers on Carbon Cloth as a Robust Hierarchical Electrocatalyst with Platinum-Comparable Activity toward Hydrogen Evolution. *ACS Applied Energy Materials*, 1(7):3143–3150, 2018. doi: 10.1021/acsaem.8b00334.

- [63] D. Löffler, J. J. Uhlrich, M. Baron, B. Yang, X. Yu, L. Lichtenstein, L. Heinke, C. Büchner, M. Heyde, S. Shaikhutdinov, H. J. Freund, R. Włodarczyk, M. Sierka, and J. Sauer. Growth and structure of crystalline silica sheet on Ru(0001). *Physical Review Letters*, 105(14):2–5, 2010. doi: 10.1103/PhysRevLett.105.146104.
- [64] Wenchang Lu, Peter Krüger, and Johannes Pollmann. *Atomic and electronic structure of (formula presented)*, volume 60. 1999. ISBN 9780521810104. doi: 10.1103/PhysRevB.60.2495.
- [65] Carolina H. Macgillavry, H. C. J. De Decker, and L. M. Nijland. Crystal Structure of the Third Form of Phosphorus Pentoxide. *Nature*, 164(4167):448–449, 9 1949. doi: 10.1038/164448b0.
- [66] Theodore E Madey, Nadir S Faradzhev, Boris V Yakshinskiy, and N V Edwards. Surface phenomena related to mirror degradation in extreme ultraviolet ( EUV ) lithography. 253:1691–1708, 2006. doi: 10.1016/j.apsusc.2006.04.065.
- [67] Sergei N. Magonov and Myung Hwan Whangbo. *Surface Analysis with STM and AFM*, volume 119. Wiley, 12 1995. ISBN 9783527293131. doi: 10.1002/9783527615117.
- [68] Oleksandr I. Malyi, Kostiantyn V. Sopiha, Claudia Draxl, and Clas Persson. Stability and electronic properties of phosphorene oxides: from 0-dimensional to amorphous 2-dimensional structures. *Nanoscale*, 9(7):2428–2435, 2017. doi: 10.1039/c6nr08810d.
- [69] Oleksandr I. Malyi, Kostiantyn V. Sopiha, Ihor Radchenko, Ping Wu, and Clas Persson. Tailoring electronic properties of multilayer phosphorene by siliconization. *Physical Chemistry Chemical Physics*, 20(3):2075–2083, 2018. doi: 10.1039/c7cp06196j.
- [70] S. Marchini, S. Günther, and J. Wintterlin. Scanning tunneling microscopy of graphene on Ru(0001). *Physical Review B - Condensed Matter and Materials Physics*, 76(7):1–9, 2007. doi: 10.1103/PhysRevB.76.075429.
- [71] M. Martin, W. Mader, and E. Fromm. Oxidation of iron, aluminium and titanium films in the temperature range 50–200 °C. *Thin Solid Films*, 250(1-2):61–66, 10 1994. doi: 10.1016/0040-6090(94)90166-X.
- [72] Maxwell, Hendricks, and Denting. unknown. *Journal of the American Chemical Society*, 1937.
- [73] K. S. Novoselov, A. K. Geim, S. V. Morozov, D. Jiang, Y. Zhang, S. V. Dubonos, I. V. Grigorieva, and A. A. Firsov. Electric Field Effect in Atomically Thin Carbon Films. *Science*, 306(5696):666–669, 10 2004. doi: 10.1126/science.1102896.
- [74] T. Okazawa, T. Nishizawa, T. Nishimura, and Y. Kido. Oxidation kinetics for Ni<sub>111</sub>... and the structure of the oxide layers. *Physical Review B*, 75(3):033413, 1 2007. doi: 10.1103/PhysRevB.75.033413.
- [75] H. Over. Ruthenium dioxide, a fascinating material for atomic scale surface chemistry. *Applied Physics A: Materials Science and Processing*, 75(1):37–44, 2002. doi: 10.1007/s003390101053.
- [76] Rudy Peeters, Sjoerd Lok, Erwin Van Alphen, Noreen Harned, Peter Kuerz, Martin Lowisch, Henk Meijer, David Ockwell, Eelco Van Setten, Guido Schiffelers, Jan-willem Van Der Horst, Carl Zeiss, and S M T Ag. ASML 's NXE platform performance and volume introduction. 8679:1–15, 2013. doi: 10.1117/12.2010932.
- [77] Yi Peng, Bingzhang Lu, Nan Wang, Jia En Lu, Chunhong Li, Yuan Ping, and Shaowei Chen. Oxygen Reduction Reaction Catalyzed by Black-Phosphorus-Supported Metal Nanoparticles: Impacts of Interfacial Charge Transfer. *ACS Applied Materials and Interfaces*, 11(27):24707–24714, 2019. doi: 10.1021/acsami.9b05471.
- [78] John P. Perdew, Kieron Burke, and Matthias Ernzerhof. Generalized gradient approximation made simple. *Physical Review Letters*, 77(18):3865–3868, 1996. doi: 10.1103/PhysRevLett.77.3865.

- [79] M. Pisarra, R. Bernardo-Gavito, J. J. Navarro, A. Black, C. Díaz, F. Calleja, D. Granados, R. Miranda, F. Martín, and A. L. Vázquez de Parga. Coverage evolution of the unoccupied Density of States in sulfur superstructures on Ru(0001). *Applied Surface Science*, 433:300–305, 2018. doi: 10.1016/j.apsusc.2017.10.069.
- [80] Edward Sanville, Steven D. Kenny, Roger Smith, and Graeme Henkelman. Improved grid-based algorithm for Bader charge allocation. *Journal of Computational Chemistry*, 28(5):899–908, 4 2007. doi: 10.1002/jcc.20575.
- [81] C. Schwennicke, D. Jürgens, G. Held, and H. Pfnür. The structure of dense sulphur layers on Ru(0001) II. The ( $\sqrt{7} \times \sqrt{7}$ ) R19.1° structure. *Surface Science*, 330(1):11–19, 1995. doi: 10.1016/0039-6028(95)00060-7.
- [82] L. Shulenburger, A. D. Baczewski, Z. Zhu, J. Guan, and D. Tománek. The Nature of the Interlayer Interaction in Bulk and Few-Layer Phosphorus. *Nano Letters*, 15(12):8170–8175, 2015. doi: 10.1021/acs.nanolett.5b03615.
- [83] D. Stachel, I. Svoboda, and H. Fuess. Phosphorus Pentoxide at 233 K. *Acta Crystallographica Section C Crystal Structure Communications*, 51(6):1049–1050, 1995. doi: 10.1107/s0108270194012126.
- [84] C. Stampfl and M. Scheffler. Theoretical study of O adlayers on Ru(0001). *Physical Review B - Condensed Matter and Materials Physics*, 54(4):2868–2872, 1996. doi: 10.1103/PhysRevB.54.2868.
- [85] P. Stampfl, S. Schwegmann, H. Over, M. Scheffler, and G. Ertl. Structure and stability of a high-coverage ( $1 \times 1$ ) oxygen phase on Ru(0001). *Physical Review Letters*, 77(16):3371–3374, 1996. doi: 10.1103/PhysRevLett.77.3371.
- [86] Martin Stöhr, Troy Van Voorhis, and Alexandre Tkatchenko. Theory and practice of modeling van der Waals interactions in electronic-structure calculations. *Chemical Society Reviews*, 48(15):4118–4154, 2019. doi: 10.1039/c9cs00060g.
- [87] P. Sutter, M. S. Hybertsen, J. T. Sadowski, and E. Sutter. Electronic structure of few-layer epitaxial graphene on Ru(0001). *Nano Letters*, 9(7):2654–2660, 2009. doi: 10.1021/nl901040v.
- [88] W. Tang, E. Sanville, and G. Henkelman. A grid-based Bader analysis algorithm without lattice bias. *Journal of Physics Condensed Matter*, 21(8), 2009. doi: 10.1088/0953-8984/21/8/084204.
- [89] Héloïse Tissot, Xuefei Weng, Philomena Schlexer, Gianfranco Pacchioni, Shamil Shaikhutdinov, and Hans Joachim Freund. Ultrathin silica films on Pd(111): Structure and adsorption properties. *Surface Science*, 678(February):118–123, 2018. doi: 10.1016/j.susc.2018.02.016.
- [90] Alexandre Tkatchenko and Matthias Scheffler. Accurate Molecular Van Der Waals Interactions from Ground-State Electron Density and Free-Atom Reference Data. *Physical Review Letters*, 102(7):7–20, 2009. doi: <https://doi.org/10.1103/PhysRevLett.102.073005>.
- [91] Charles M. Truong, José A. Rodriguez, and D. Wayne Goodman. Molecular precursors to boron nitride thin films. 2. Coadsorption and reaction of hydrazine and diborane on Ru(0001). *Journal of Physical Chemistry*, 96(1):341–347, 1992. doi: 10.1021/j100180a063.
- [92] B. Turkot, S. Carson, and A. Lio. Continuing Moore’s law with EUV lithography. In *2017 IEEE International Electron Devices Meeting (IEDM)*, pages 1–14. IEEE, 12 2017. ISBN 978-1-5386-3559-9. doi: 10.1109/IEDM.2017.8268390.
- [93] Martin Uhrin. Allotropes of phosphorus, 2021.
- [94] Michel A. Van Hove, William H. Weinberg, and Chi-Ming Chan. *Low-Energy Electron Diffraction*, volume 6 of *Springer Series in Surface Sciences*. Springer Berlin Heidelberg, Berlin, Heidelberg, 1986. ISBN 978-3-642-82723-5. doi: 10.1007/978-3-642-82721-1.

- [95] John R. Van Wazer. Phosphorus and its compounds. *interscience publishers, inc.*, 23(82):50–50, 1958. doi: 10.1177/019263653902308210.
- [96] Lorena Vega, Judit Ruvireta, Francesc Viñes, and Francesc Illas. Jacob's Ladder as Sketched by Escher: Assessing the Performance of Broadly Used Density Functionals on Transition Metal Surface Properties. *Journal of Chemical Theory and Computation*, 14(1):395–403, 2018. doi: 10.1021/acs.jctc.7b01047.
- [97] Elena Voloshina and Yuri Dedkov. Atomic force spectroscopy and density-functional study of graphene corrugation on Ru (0001). 235418:1–6, 2016. doi: 10.1103/PhysRevB.93.235418.
- [98] Carl Wagner. Beitrag zur Theorie des Anlaufvorgangs. *z. physikal. Chem.*, B(21):25–41, 1933.
- [99] M. Mitchell Waldrop. MORE THAN MOORE. *nature*, 530:144–147, 2016.
- [100] B. Wang, M. L. Bocquet, S. Günther, and J. Wintterlin. Comment on "periodically rippled graphene: Growth and spatially resolved electronic structure". *Physical Review Letters*, 101(9):99703, 2008. doi: 10.1103/PhysRevLett.101.099703.
- [101] B. Wang, M. L. Bocquet, S. Marchini, S. Günther, and J. Wintterlin. Chemical origin of a graphene moiré overlayer on Ru(0001). *Physical Chemistry Chemical Physics*, 10(24):3530–3534, 2008. doi: 10.1039/b801785a.
- [102] B. Wang, S. Günther, J. Wintterlin, and M. L. Bocquet. Periodicity, work function and reactivity of graphene on Ru(0001) from first principles. *New Journal of Physics*, 12(111), 2010. doi: 10.1088/1367-2630/12/4/043041.
- [103] Gaoxue Wang, Ravindra Pandey, and Shashi P. Karna. Phosphorene oxide: Stability and electronic properties of a novel two-dimensional material. *Nanoscale*, 7(2):524–531, 2015. doi: 10.1039/c4nr05384b.
- [104] Q. Wang, D. Gilmer, Yue Fan, A. Franciosi, D. F. Evans, and W.L. Gladfelter. Microstructure of ruthenium dioxide films grown on  $\text{Al}_2\text{O}_3(0001)$ ,  $\text{Al}_2\text{O}_3(1\ 1\ 02)$ , and  $\text{SrTiO}_3(100)$  using reactive sputtering. *Journal of Materials Research*, 12(4):984–998, 1997. doi: 10.1016/S0169-4332(02)00802-4.
- [105] Fengnian Xia, Han Wang, and Yichen Jia. Rediscovering Black Phosphorus: A Unique Anisotropic 2D Material for Optoelectronics and Electronics. 2 2014. doi: 10.1038/ncomms5458.
- [106] Tatsuya Yanagida, Hitoshi Nagano, Yasunori Wada, Takayuki Yabu, Shinji Nagai, Georg Soumagne, Tsukasa Hori, Kouji Kakizaki, Akira Sumitani, Junichi Fujimoto, Hakaru Mizoguchi, and Akira Endo. Characterization and optimization of tin particle mitigation and EUV conversion efficiency in a laser produced plasma EUV light source. *Extreme Ultraviolet (EUV) Lithography II*, 7969(April 2011):79692T, 2011. doi: 10.1117/12.879189.
- [107] Min Yu and Dallas R. Trinkle. Accurate and efficient algorithm for Bader charge integration. *Journal of Chemical Physics*, 134(6):1–8, 2011. doi: 10.1063/1.3553716.
- [108] Andrew Zangwill. The education of Walter Kohn and the creation of density functional theory. *Archive for History of Exact Sciences*, 68(6):775–848, 2014. doi: 10.1007/s00407-014-0140-x.
- [109] Hui Zhang, Qiang Fu, Yi Cui, Dali Tan, and Xinhe Bao. Growth mechanism of graphene on Ru(0001) and O<sub>2</sub> adsorption on the graphene/ Ru(0001) surface. *Journal of Physical Chemistry C*, 113(19):8296–8301, 2009. doi: 10.1021/jp810514u.
- [110] Yuanmeng Zhao, Xuwei Wang, Gongzhen Cheng, and Wei Luo. Phosphorus-Induced Activation of Ruthenium for Boosting Hydrogen Oxidation and Evolution Electrocatalysis. *ACS Catalysis*, 10(20):11751–11757, 2020. doi: 10.1021/acscatal.0c03148.
- [111] Carlos Fernando Zinola. Density functional theory. *Electrocatalysis: Computational, Experimental, and Industrial Aspects*, pages 117–138, 2010. doi: 10.1201/9781420045451.